Ref. Ares(2020)6135474 - 30/10/2020

TRI-HP PROJECT

Trigeneration systems based on heat pumps with natural refrigerants and multiple renewable sources

Experimental results of a tri-partite gas cooler

Deliverable number: D4.3

Version 1.0

Funded by the European Union's Horizon 2020 research and innovation programme under grant agreement N. 814888. The sole responsibility for the content of this paper lies with the authors. It does not necessarily reflect the opinion of the European Commission (EC). The EC is not responsible for any use that may be made of the information it contains.

This page is intentionally left blank

Project Acronym:	TRI-HP
Project URL:	http://www.tri-hp.eu
Editor:	Alireza Zendehboudi, NTNU
Deliverable nature:	Report (R)
Dissemination level:	Public (PU)
Contractual Delivery Date:	September 30, 2020
Actual Delivery Date	October 30, 2020
Number of pages:	40
Keywords:	Heat pumps, transcritical cycle, carbon dioxide, tri-partite gas cooler, experimental study
Authors:	Alireza Zendehboudi (NTNU), Ángel Álvarez Pardiñas (NTNU)
Peer review:	Daniel Carbonell (SPF-HSR), Raphael Gerber (CADENA/HEIM)
Approval:	Daniel Carbonell (SPF-HSR)

Revision History

Date	Version	Changes
October 30, 2020	v1.0	First version submitted to EC

TRI-HP CONSORTIUM

SPF INSTITUT FÜ SOLARTECHI HSR	Oberseestrasse 10 CH-8640 Rapperswil, Switzerland	Dr. Daniel Carbonell Dani.Carbonell@spf.ch
tecnalia Inspiring Business	Área Anardi, 5. E-20730 Azpeitia (Gipuzkoa), Spain	Mr. Andoni Diaz de Mendibil andoni.diazdemendibil@tecnalia. com
cadena	Murtenstrasse 116, CH-3202, Frauenkappelen, Switzerland	Mr. Raphael Gerber raphael.gerber@cadena.ch
IREC 10	Jardins de les Dones de Negre 1 2ªpl. 08930 Sant Adrià de Besòs (Barcelona)	Dr. Jaume Salom jsalom@irec.cat
ALFA LAVAL	Box 74, 22100 Lund, Sweden	Mr Mats Nilsson MatsR.Nilsson@alfalaval.com
ILAG swiss quality coatings	Hämmerli 1, CH-8855, Wangen, Switzerland	Mrs. Stephanie Raisch stephanie.raisch@ilag.ch
Institut für sozial-ökologische Forschung	Hamburger Allee 45, Frankfurt am Main, 60486, Germany	Dr. Immanuel Stiess stiess@isoe.de
NTNU Norwegian University of Science and Technology	Kolbjørn Hejes vei 1D (B249), No-034 Trondheim, Norway	Dr. Ángel Álvarez Pardiñas angel.a.pardinas@ntnu.no
DANISH TECHNOLOGICAL INSTITUTE	Kongsvang Allé 29, 8000 Aarhus C, Denmark	Mr Claus Bischoff claus.bischoff@gmail.com
IKKU Institut für Kälte-, Klima- und Umwelttechnik Hochschule Karlsruhe Technik und Wirtschaft	Moltkestr. 30, 76133 Karlsruhe, Germany	Dr. Prof. Michael Kauffeld Michael.Kauffeld@hs-karlsruhe.de
REHVA Federation of European Heating, Ventilation and Air Conditioning Associations	Rue Washington 40, 1050 Brussels, Belgium	Ms. Anita Derjanecz ad@rehva.eu
GRUPO E.F.C. EQUIPOS FRIGORIFICOS COMPACTOS,S.L.	C/Zuaznabar 8 Pol. Ind. Ugaldetxo, Oiartzun, 20180, Spain	Mr. Gabriel Cruz g.cruz@equiposfrigorificoscompactos.com

Contents

Executive Summary

An experimental investigation on the performance of a tri-partite brazed plate gas cooler in a transcritical carbon dioxide (CO_2) heat pump water heater system is conducted. The gas cooler under investigation is partitioned to separately serve the functions of domestic water preheating, space heating, and domestic water reheating. The gas cooler is studied at a steady state for only space heating (SH) operation, only domestic hot water (DHW) operation, and simultaneous space heating and domestic hot water (DHW+SH) operation. Measurements are performed for counterflow configuration with two different internal arrangements: (i) three individual single-pass heat exchangers with a U configuration and (ii) a two-pass arrangement for preheating and reheating domestic hot water. The heat pump unit is designed with a heat duty of 10 kW, 8 kW, and 10 kW under DHW, SH, and DHW+SH modes to provide the tap water heating and space heating water up to 70 °C and 35 °C, respectively. The effects of inlet pressure, CO_2 and water mass flow rates, and water inlet temperature on the total heat transfer coefficient, heat duty, pressure drop, supply temperature, and temperature approach are analyzed in detail. To present a reference for brazed plate gas cooler optimization design in transcritical CO_2 systems, the heat duty and supply temperature correlations for both space heating and domestic hot water cycles are also developed and validated with experimental data.

As shown by the experimental results, the gas cooler shows promising performance and is more compact than previous designs. Under the design conditions, the heat duty meets the requirements to provide the supply temperatures of 35 °C and 70 °C for the space heating and tap water heating applications. The pressure drops in the tri-partite gas cooler are low under different operating modes and the temperature approaches for the reheating gas cooler vary between 6.52 K and 8.24 K under design conditions in DHW+SH and DHW modes, depending on the internal heat exchanger arrangement. This value is 0.65 K for the SH operating condition. This shows that CO_2 liquid phase enters the throttling device, indicating good performance of the evaluated gas cooler.

It is found that the operating pressure has a considerable impact on the heat transfer coefficients in the near-critical region. The maximum of heat transfer appears at the region in the vicinity of the pseudo-critical point and the peak point of the heat transfer coefficient shifts to the high-temperature state when the operating gas cooler pressure increases. Furthermore, no significant and clear influence of the water inlet temperature is demonstrated on the heat transfer coefficients when CO_2 is in a high-temperature state. The values of heat duty increases with the increases of water and CO_2 mass flow rates. The lower the water inlet temperature is, the higher the average heat duty is. Increase of CO_2 mean temperature flowing through the gas cooler causes a decrease in the density and viscosity of the refrigerant to maintain the flow continuity, resulting in a larger Reynolds number and then pressure drop. The increase in the hot side fluid pressure can cause an increase in the density and thus a decrease in the velocity of CO_2, so the CO_2 side pressure drop decreases. A larger mass flow rate of refrigerant and a lower water mass flow rate increases the water supply temperature. The higher water mass flow rate is recommended to decrease the temperature approach values under DHW, SH, and DHW+SH operations. Ultimately, the values of coefficient of determination for the reheating heat duty, space heating heat duty, preheating heat duty, DHW supply temperature, and SH supply temperature are 0.88, 0.86, 0.94, 0.99, and 0.94, respectively. The results show that the correlations perform very well in the prediction of heat duty and supply temperature. The basic data for the characteristics of CO_2 in the present experimental study are of significance in designing and optimizing the transcritical CO_2 systems.

NOMENCLATURE

Acronyms

COP	coefficient of performance
DHW	domestic hot water
GP	Genetic Programming
LMTD	logarithmic mean temperature difference
SH	space heating

Symbols

A	heat transfer area (mm^2)
CO_2	carbon dioxide
c_{P,H_2O}	specific heat of water (kJ/kg.K)
H_2O	water
$h_{CO_2,in}$	enthalpy of CO_2 at the inlet (kJ/kg)
$h_{CO_2,out}$	enthalpy of CO_2 at the outlet (kJ/kg)
HPV	high-pressure electronic expansion valve
HX1	reheating gas cooler
HX2	space heating gas cooler
HX3	preheating gas cooler
m_{CO_2}	CO_2 mass Flow rate (kg/min)
m_{H_2O}	water mass flow rate (kg/min)
$Q_{average}$	average heat duty (kW)
Q_{CO_2}	CO_2 heat duty (kW)
Q_{H_2O}	water heat duty (kW)
R^2	coefficient of determination
T5	DHW inlet temperature (°C)
T8	SH inlet temperature (°C)

T_b	average bulk fluid temperature (°C)
$T_{H_2O,in}$	temperature of water at the inlet (°C)
$T_{H_2O,out}$	temperature of water at the outlet (°C)
T_{SC}	pseudo-critical temperature (°C)
U_{total}	total heat transfer coefficient (kW/m^2.°C)

Greek Symbols

Δ P	pressure drop (bar)
$\Delta T_{approach}$	temperature approach (K)

1 Introduction

The hydrofluorocarbons (HFCs) refrigerants used as working fluids in vapor compression systems can increase the greenhouse effect. For example, R134a with a high global warming potential (GWP) of 1300 is used in a wide range of refrigeration and air conditioning systems [1]. The clear phase-out pathway of HFCs is listed in the Kigali amendment report to contribute to the goal of the international climate agreement to avoid a 0.5 °C increase of the global mean surface temperature by 2100 [2].

The use of natural and environmentally friendly refrigerants, such as air, hydrocarbons, water, ammonia, and carbon dioxide (CO_2), has attracted much attention to mitigate the greenhouse gas emissions from refrigeration, air-conditioning, and heat pumping systems [3]. Several drop-ins and retrofit experimental tests have been performed during the past years to improve the knowledge of the behavior of these fluids in real operation. CO_2 as a non-flammable fluid is a promising candidate and is seen as an excellent alternative to synthetic refrigerants. CO_2 has a negligible global warming potential (GWP=1), low cost, zero ozone depletion potential, high availability, and is safe and non-toxic [4]. No other refrigerant meets these properties simultaneously. Due to the low critical pressure and temperature of CO_2 (73.7 bar and 31.1 °C), Lorentzen and Pettersen [5] from NTNU-SINTEF laboratory introduced the application of transcritical CO_2 system in the mobile air-conditioning to resolve the efficiency problem of subcritical cycles near the critical point.

Figure 1.1 shows various CO_2 thermophysical properties as a function of temperature at different pressures of 80, 85, 90, 95, and 100 bar. The physical properties are obtained from REFPROP, Version 10. At a specific pressure, the temperature at which the specific heat of CO_2 reaches a peak is called the pseudo-critical point (Figure 1.1 (b)). The physical properties of supercritical CO_2 vary significantly with the temperature around its critical point. For example, the specific heat of CO_2 reaches a maximum value near critical temperature for all considered pressures. The peak value of specific heat decreases as the pressure increases. The density and viscosity show sharp downward trends with an increase in temperature. At one particular temperature, small temperature variation causes a sharp drop in their values, and the curves become nearly vertical for the lower pressures. A similar trend is observed for the thermal conductivity. The thermal conductivity of CO_2 reaches a peak value for pressures near-critical pressure and then becomes a flat line at high temperatures. All these thermophysical properties significantly affect the design and optimization of gas coolers at supercritical conditions.

The transcritical CO_2 heat pump system is a promising technology for heating of tap water with high temperature [6]. In a transcritical CO_2 system, the heat-absorbing process occurs below the critical point while the heat rejection process takes place above the critical point. The difference between inlet temperature and outlet temperature of CO_2 in a gas cooler, known as temperature glide, can be much higher than in a condensing process in a traditional heat pump water heater. A heat pump water heater using CO_2 as a refrigerant can take the advantage of high temperature glide of CO_2 when it is cooled down from a vapor-like region to a liquid-like region in a gas cooler. In a counter-flow arrangement, the water temperature can rise to the desired value for the space heating and tap water heating applications [7]. Therefore, such temperature glide matching between the hot and cold streams in a gas cooler can enhance the performance of a CO_2 heat pump system and decrease the generation of entropy in the gas cooler unit [8].

Neksa, et al. [9] experimentally evaluated the performance of a 50 kW CO_2 heat pump water heater at the laboratory of NTNU-SINTEF Energy. The experimental results indicated that when the evaporating temperature was 0 °C, the water temperature could be heated from 9 °C to 60 °C and the coefficient of heat pump could reach 4.3. Besides, the evaluated system energy consumption could be decreased by 75% compared to the electric water heater and gas water heater. Nekså [10] discussed the important characteristics of transcritical CO_2 heat pumps and exploited

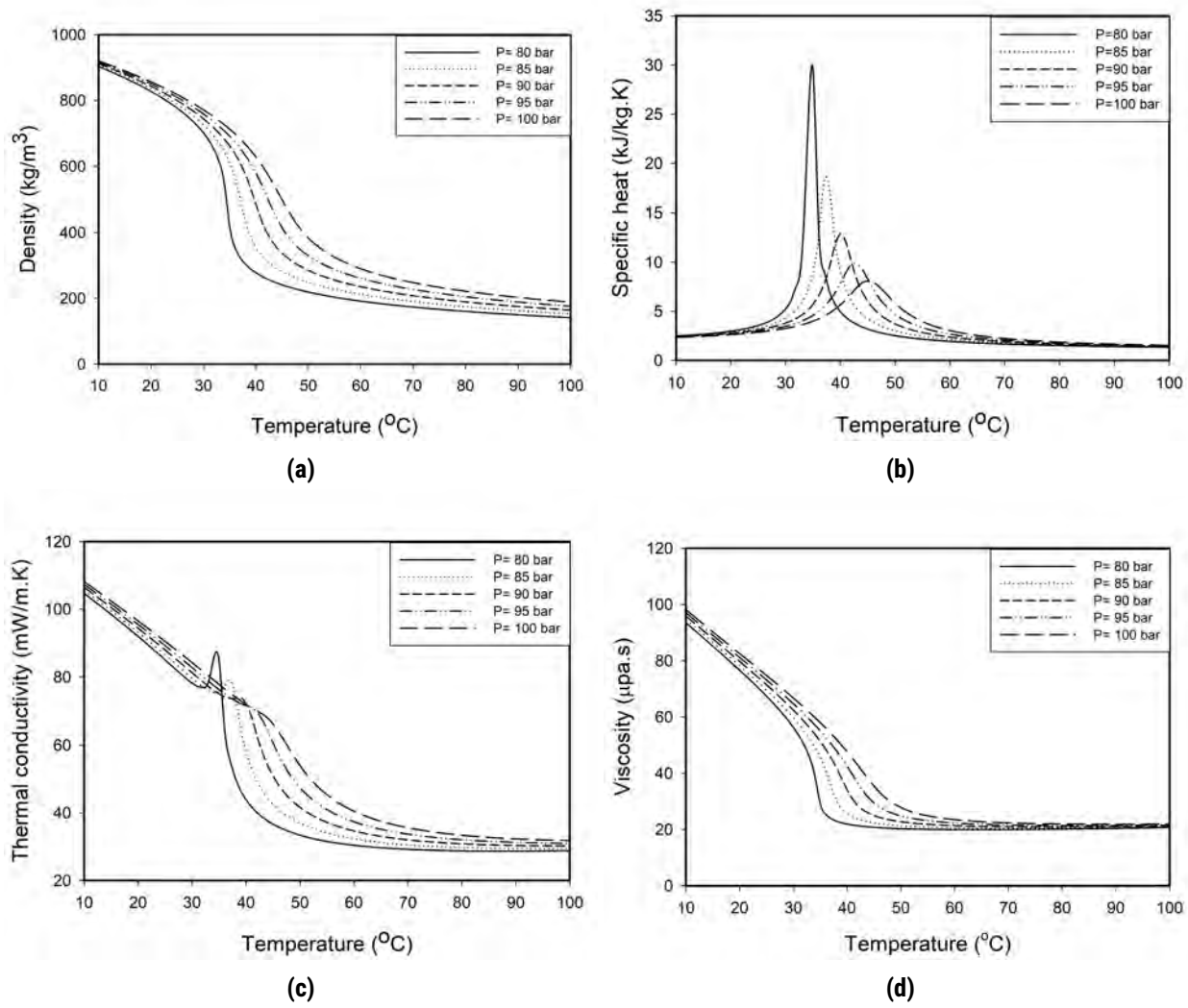

Figure 1.1: Thermophysical properties of CO_2 at different pressures: (a) density; (b) specific heat; (c) thermal conductivity; (d) viscosity.

specific characteristics of the fluid and the transcritical process. The results showed that CO_2 was an attractive alternative to synthetic fluids. White et al. [11] constructed a transcritical CO_2 heat pump prototype for heating tap water to temperatures higher than 65 °C using shell and tube gas coolers. The heating capacity and heating coefficient of performance were 115 kW and 3.4, respectively, for providing the hot water temperature of 77.5 °C. Stene [12] considered helical counter-flow tube-in-tube gas coolers and carried out experiments on a dual function heat pump water heater. For the first time in the literature, the gas cooler was partitioned to separately serve the functions of domestic water preheating, space heating, and domestic water reheating. The COP was highest for the combined mode operation, slightly lower for only domestic water heating, and lowest for only space heating operation. Sarkar et al. [13] theoretically analyzed a system designed for simultaneous heating and cooling of water. One stream of water served as the heat source and was thus cooled by the evaporator. The second stream of water served as the heat sink and was thus heated in the gas cooler. The two water streams entered the respective heat exchangers at the same temperature. Minetto [14] described the development of a CO_2 air/water

heat pump to produce tap hot water in a residential building. A control method was developed to maximize the COP of the tested heat pump system. The tube-in-tube heat exchanger was used to carry out the experiments. Wang et al. [15] evaluated the performance of an air-source heat pump water heater with tube-in-tube type gas cooler under a low ambient temperature of -15 °C. The transcritical CO_2 heat pump water heater was proved to be a promising solution for providing hot water temperature of 80 °C at a fixed water inlet temperature of 12 °C. Zhu et al. [16] investigated the effects of different operating parameters on the performance of a transcritical CO_2 ejector–expansion heat pump water heater system for tap water outlet temperatures ranging from 50 to 90 °C. The gas cooler was a tube-in-tube heat exchanger with water as the coolant. The coefficient of performance of the ejector–expansion heat pump system reached 4.6 when the tap water outlet temperature was 70 °C. Recently, Smitt et al. [17] studied the performance of an integrated CO_2 heat pump and chiller unit in a Norwegian hotel for one year. The system was designed to supply heat for ventilation heating, domestic hot water, and space heating. The system was able to provide hot water up to 70 °C with high efficiency.

The performance of the gas cooler is one of the key factors in a transcritical CO_2 heat pump water heater system. The performance of the gas cooler is affected by many factors, such as the water inlet temperature, operating pressure, mass flow rates, and style of a heat exchanger. To improve the performance of the gas cooler in a transcritical CO_2 system, many specific studies have been conducted. Pettersen et al. [18] reviewed the unique characteristics of heat exchangers used for CO_2 in evaporators and gas coolers. Sarkar et al. [19] analyzed the irreversibilities of the gas cooler and concluded that approximately 90% of the heat exchanger losses were due to temperature differences between the refrigerant and the secondary fluid. Later, Sarkar et al. [20] developed a theoretical methodology to perform the optimization of tube-in-tube heat exchanger geometry based on minimizing irreversibility. An experimental study by Fronk and Garimella [21] studied the performance of three different microchannel CO_2 gas coolers under varying operating conditions.

The heat transfer characteristics and pressure drops of CO_2 at supercritical pressures are important for the efficiency improvement of gas coolers. Pitla et al. [22] experimentally and numerically studied the heat transfer and pressure drop of supercritical CO_2 in a tube with an inner diameter of 4.72 mm. Dang and Hihara [3] experimentally researched the heat transfer of supercritical CO_2 in horizontal circular tubes with diameters between 1 mm and 6 mm. Son and Park [23] made a test facility to experimentally investigate the heat transfer and pressure drop characteristics of supercritical CO_2 in a horizontal tube with a diameter of 7.75 mm. Liu et al. [24] conducted experiments to measure the heat transfer and pressure drop of supercritical CO_2 in large tubes with diameters of 4, 6, and 10.7 mm. Ma et al. [25] conducted an experimental investigation to evaluate the heat transfer coefficient of supercritical CO_2 near the pseudo-critical temperature in a double pipe heat exchanger with 25 mm outer diameter and 16 mm inner diameter. Zhang et al. [26] experimentally and numerically studied the heat transfer and pressure drop of supercritical CO_2 flowing through horizontal tubes with inner diameters from 4 mm to 10 mm. Zhu et al. [27] experimentally studied the heat transfer characteristics of CO_2 at supercritical pressures during cooling in two fluted tube-in-tube heat exchangers and a smooth tube-in-tube heat exchanger. Both the overall heat transfer and the local heat transfer coefficients were investigated at various CO_2 mass flow rates, inlet pressures, and flute pitches.

The gas cooler design needs a special consideration due to the high operating pressure and temperature glide in a transcritical CO_2 heat pump water heater system. Improvements to the gas cooler lead to a lower temperature approach and higher CO_2 enthalpy difference across the gas cooler, resulting in a higher cycle performance. The brazed plate heat exchanger can be a promising technology for making transcritical CO_2 heat pumps reasonably efficient. The brazed plate heat exchanger is specifically designed to work in the refrigeration applications where the pressure requirements are extremely high. Brazing omits the requirement of either gaskets or frames and results in a very compact exchanger. Due to the high heat transfer coefficients, counter-flow designs, and the

lack of bypass and leakage streams, the surface area required for a plate exchanger is much lower than that of a tube-in-tube heat exchanger for a given heat duty, hence decreasing the overall cost, size, and space required for the exchanger. Therefore, experimental investigations for detailed knowledge of supercritical CO_2 in the brazed plate heat exchanger are essential.

Based on the reviewed research works, it can be concluded that the characteristics of supercritical CO_2 in tube-in-tube gas coolers have been substantially investigated under different conditions. The characteristics of supercritical CO_2 in brazed plate heat exchangers have not been experimentally reported yet. Due to lack of reported experimental works, a test setup has been built in this study to investigate the effects of operating parameters on characteristics of CO_2 flowing in a tri-partite brazed plate gas cooler. The tri-partite gas cooler is partitioned to separately serve the functions of domestic water preheating, space heating, and domestic water reheating. This approach allowed to most closely match the temperature profile of water and CO_2 through the gas cooler. Experimental data are collected for only space heating (SH) operation, only domestic hot water (DHW) operation, and simultaneous domestic hot water and space heating (DHW+SH) operation. The current research is a contribution to identify the characteristics of CO_2 in brazed plate heat exchangers.

2 Experimental apparatus and precedures

2.1 Test facility

The primary focus of this investigation is on the performance evaluation of tri-partite gas coolers. The tri-partite gas cooler consists of three brazed plate heat exchangers developed by ALFA LAVAL. The tri-partite gas cooler is placed right after the compressors. A bypass over the tri-partite gas cooler loop is installed to conduct the study separately and to be able to control the mass flow precisely. Figure 2.1 is a schematic diagram of the tri-partite gas cooler test facility. The test facility (Figure 2.1) is located at Norwegian University of Science and Technology NTNU (in Trondheim, Norway) for the evaluation of the tri-partite gas cooler. The detailed information of these heat exchangers in the experiments are summarized in Table 2.1. HX1 is used for reheating the domestic hot water to the required temperatures, HX2 heats water for space heating, and HX3 preheats the domestic hot water. All these heat exchangers fall into the counter-flow category as the CO_2 working fluid flows into the opposite direction of the water. The CO_2 gas from the MT compressor flows through the flowmeter and enters HX1 where DHW gets reheated. The CO_2 gas then enters HX2 where it heats water for space heating. T8 is the temperature of the cold incoming water into the HX2. Further, CO_2 exchanges heat into HX3 to preheat DHW which is entering at the temperature of T5 into the HX3.

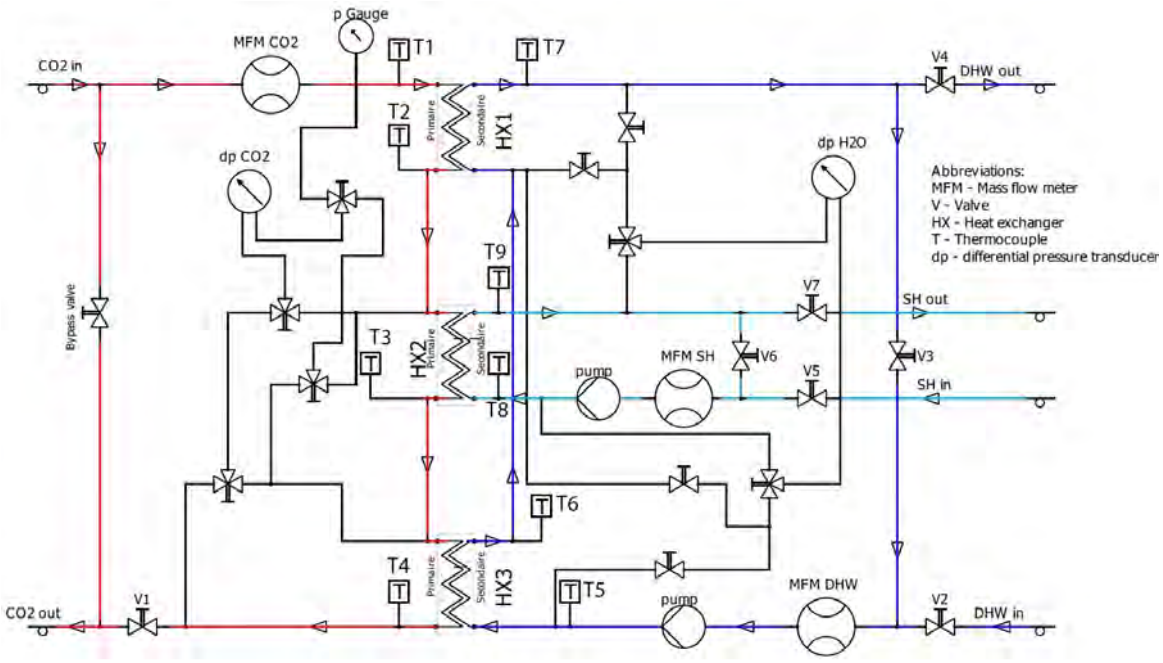

Figure 2.1: Schematic diagram of the tri-partite gas cooler.

Two different gas cooler internal arrangements are tested. The first design is the most manageable type of arrangement of heat exchangers, known as single pass, in which the CO_2 and water as fluids make just one pass, therefore there is no change in the direction of the steams. The most popular flow arrangement in a 1-pass heat exchanger is U shape. This design provides all fluid ports to be placed in the front or rare cover plate. Two-pass arrangements are also utilized in domestic hot water operation. The directions of the streams change throughout the heat exchanger and the fluids flow two times through the heat transfer surface within the heat exchanger.

Table 2.1: Detailed information of the gas coolers.

Number	Name	Length *Width (mm)	Weight (kg)	Number of plate	Arrangement
1	Reheating	190*76	1.68	34H	1-pass
2	Reheating	190*76	1.68	2*8H/1*8H+1*9H	2-pass
3	Space heating	190*76	2.32	50H	1-pass
4	Preheating	190*76	0.88	14H	1-pass
5	Preheating	190*76	0.88	2*3H/1*3H+1*4H	2-pass

In a 2-pass arrangement, the ports are placed on both cover plates. The difference between a single-pass and two-pass unit is indicated in Figure 2.2.

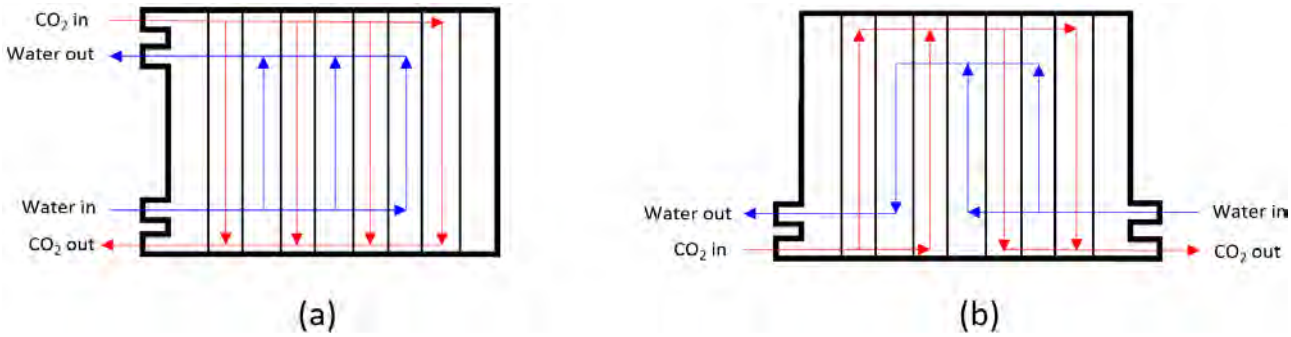

Figure 2.2: (a) single-pass and (b) two-pass arrangements inside brazed plate heat exchanges.

Each of the water loops, namely SH loop and DHW loop, consists of a pump and several valves to control the water temperature supplied to the heat exchangers. The water inlet temperature can be controlled by the returning stream of warm water on each side of the cycle. If a higher inlet temperature of DHW is required, one can open a two-way valve (V3) to mix the warm water with the cold inlet water. The same principle applies to the SH cycle by regulating valve 6. The DHW mass flow can be controlled by regulating V2 and V3. V5 and V6 have been placed to regulate the SH mass flow rate. The positions of the valves are not only dependent on the mass flow, but on the required inlet temperature as well.

The gas coolers are evaluated in a prototype CO_2 heat pump system. Figure 2.3 indicates the experimental apparatus for the performance evaluation test. The test facility unit is a comprehensive test rig with many possibilities of experimental investigations involving testing a large range of system configurations and conditions. The refrigerant cycle of the test rig consists of three piston-type compressors (Dorin CD380H and CD1000H as parallel machines and Dorin CD1400H used as the base-load machine which is a medium-temperature compressor). The evaporators are medium temperature evaporators where the pressure level is monitored by two metering expansion valves Danfoss CCM20. The system also has two Danfoss CCMT8 as the flash valve and the high-pressure valve. The suction accumulator also referred to as a liquid receiver is a 50-L vessel that delivers saturated or superheated vapor to the suction side of the medium temperature compressor, where it is compressed to a set discharge pressure. The two parallel compressors compress the gas from the liquid separator which is also a 50-L pressure receiver tank. The saturated liquid from the liquid separator gets delivered to the evaporator. Both the pressure tanks, the liquid receiver, and the liquid separator are provided with two Danfoss AKS 4100 coaxial liquid level sensors connected to the control system to secure the liquid CO_2 in the receivers. In case, the parallel

compressors are not needed, the system has a flash valve which throttles the vapor from the liquid receiver tank. The pressure level in the receiver is controlled by either the flash valve or parallel compressors. There are two internal heat exchangers, where the heat exchange between the vapor phase of CO_2 from the receivers and the high-pressure CO_2 after the gas cooler section takes place to ensure the safety of the compressors. The high-pressure CO_2 after the gas cooler can be expanded in two ways, either by a high-pressure electronic expansion valve (HPV) or by an integrated multi-ejector pack (a prototype manufactured by Danfoss) with the support of an HPV.

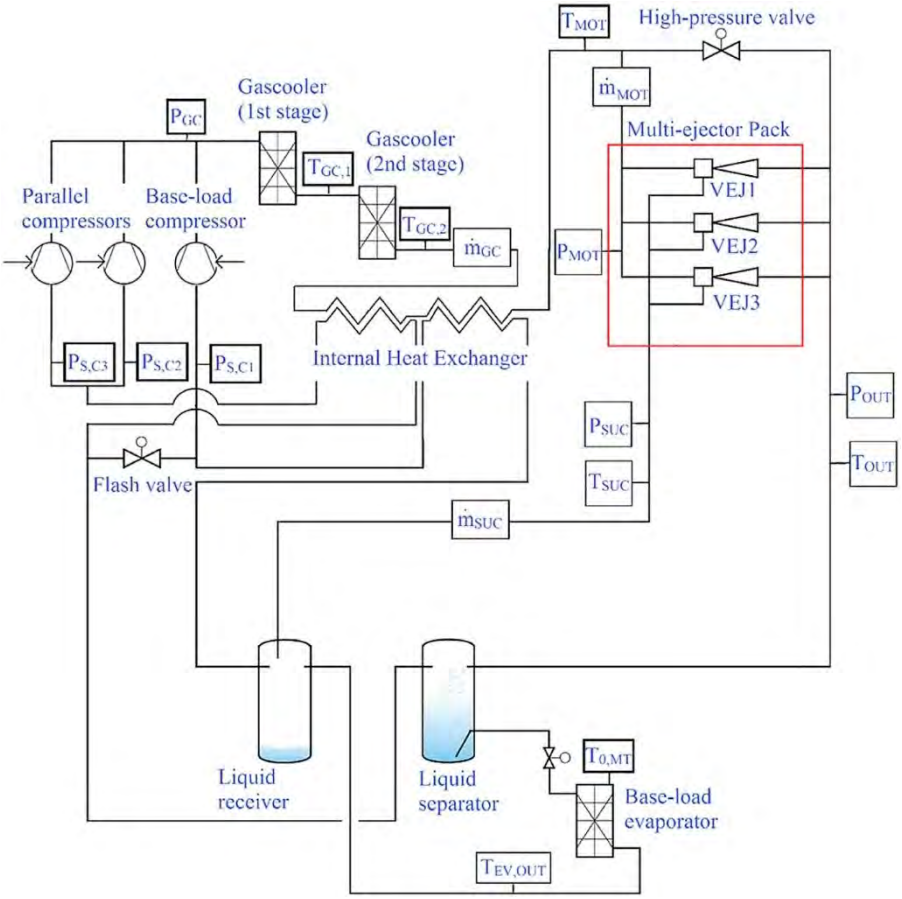

Figure 2.3: P&ID diagram of CO_2 loop in R744 multi-ejector test rig.

2.2 Measurement and control

To evaluate, control, and ensure the safety of the system, the test facility is equipped with pressure sensors, temperature sensors and mass flow meters. The measuring points for the performance evaluation test are indicated in Figure 2.1. The output signals from all the sensors are processed and communicated by the Danfoss control unit to the Danfoss Minilog system (live recording software). The inlet pressures of CO_2 are measured using the Cerabar PMP71 digital pressure transmitter with a metallic membrane with an uncertainty level of ±0.25% in the set span. The pressure drops in water and CO_2 sides are measured using the Deltabar PMD75 differential pressure transmitter with a piezoresistive sensor and welded metallic membrane with an accuracy of ±0.25% in the set span. The temperatures of CO_2 and water at the inlet and outlet of gas coolers are measured by Pt 1000 sensor with an accuracy of ±0.15 °C at 0 °C. In addition, the DHW flow rate is measured by FLR 1000 sensor with an

accuracy of ±3% in the full span, and CO_2 and SH flow rates are measured by Rheonik RHM 08 Coriolis flow meter type of sensor with an accuracy of ±0.1% of reading.

2.3 Test conditions

In the present experimental study, the data are measured for various gas cooler pressures, discharge temperatures, CO_2 mass flow rates, CO_2 inlet and outlet temperatures, water mass flow rates, water inlet and outlet temperatures and pressure drops. The one-pass DHW gas coolers are tested under different operating conditions. In order to plot curves of different parameters, Table 2.2 summarizes the experimental conditions for SH gas cooler and two-pass DHW gas coolers.

Table 2.2: Experiment conditions.

Run #	Pressure (bar)	Discharge temperature (°C)	DHW inlet temperature (°C)	SH inlet temperature (°C)	DHW mass flow rate (kg/min)	SH mass flow rate (kg/min)	CO_2 mass flow rate (kg/min)
DHW operation							
1	94	97	16	-	1.8/2/2.2/2.4/2.6	-	2.15
2	94	97	13.1	-	1.8/2/2.2/2.4/2.6	-	2.15
3	100	97	13.1	-	1.8/2/2.2/2.4/2.6	-	2.15
4	100	97	13.1	-	1.8/2/2.2/2.4/2.6	-	2.4
SH operation							
5	85	76	-	30	-	21.8/22.8/23.8/24.8	2.4
6	90	76	-	30	-	21.8/22.8/23.8/24.8	2.4
7	90	76	-	35	-	21.8/22.8/23.8/24.8	2.4
8	90	76	-	35	-	21.8/22.8/23.8/24.8	1.85
9	90	76	-	35	-	21.8/22.8/23.8/24.8	2.6
10	90	76	-	35	-	21.8/22.8/23.8/24.8	2.2
11	90	76	-	25	-	21.8/22.8/23.8/24.8	2.4
DHW+SH operation							
12	85	80	12.6	30	1.3	21.8	1.88/2/2.2/2.35/2.6
13	85	80	12.6	30	1.3	24.8	1.88/2/2.2/2.35/2.6
14	90	80	12.6	30	1.3	15/17/21.7/24.8	2.4
15	85	80	12.6	30	1.3	15	1.8/2/2.2/2.35/2.6
16	80	80	12.6	30	1.3	15/17/21.7/24.8	2.4
17	90	80	12.6	25	1.3	11.6/15/17/21.7/24.8	2.4
18	90	80	12.8	30	1/1.45/2/2.5	11.5	2.4
19	90	80	17.8	30	1/1.5/2/2.5	11.5	2.4
20	90	80	12.8	30	1.2/1.5/2/2.5	11.5	1.7
21	80	80	12.8	30	1.09/1.5/2/2.5	11.5	2.4

3 Data reduction

To study the heat transfer coefficient, the reduction of the experimental data is performed as follows. The CO_2 heat duty, Q_{CO_2}, and water heat duty, Q_{H_2O}, can be calculated using Equations 3.1 and 3.2, respectively.

$$Q_{CO2} = m_{CO2} \times (h_{CO2,in} - h_{CO2,out}) \tag{3.1}$$

$$Q_{H2O} = m_{H2O} \times c_{p,H2O} \times (T_{H2O,out} - T_{H2O,in}) \tag{3.2}$$

where m_{CO_2} is the CO_2 mass Flow rate, m_{H_2O} is the water mass flow rate, $h_{CO_2,in}$ and $h_{CO_2,out}$ are the enthalpy of CO_2 at the inlet and outlet of a gas cooler in the CO_2 side, respectively, $T_{H_2O,out}$ and $T_{H_2O,in}$ are the symbols of the water temperature at the outlet and inlet of a gas cooler in the water side,respectively, and c_{P,H_2O} is the specific heat of water. The CO_2 enthalpy is determined as functions of temperature and pressure using REFPROP, Version 10.0 [28].

For all three gas coolers, the energy balance between Q_{H_2O} and Q_{CO_2} is calculated, and the maximum relative deviation is less than 5%. The comparison of the calculated data indicates that there is an energy balance between CO_2 and H_2O sides. The total heat transfer coefficient, U_{total}, of a gas cooler is calculated from the average of the heat duties and logarithmic mean temperature difference, as:

$$U_{total} = \frac{Q_{average}}{A \times LMTD} \tag{3.3}$$

where $Q_{average}$ is the average heat duty, A is the heat transfer area, and LMTD is the logarithmic mean temperature difference. The average heat duty is calculated by:

$$Q_{average} = \frac{Q_{CO2} + Q_{H2O}}{2} \tag{3.4}$$

In the supercritical region, the specific heat of CO_2 varies significantly in the vicinity of the pseudo-critical point. Hence, the calculated U_{total} value in this investigation is an approximation to compare the values under the same gas cooler geometry and condition. Thus, the logarithmic mean temperature difference is used and calculated as:

$$LMTD = \frac{(T_{CO2,out} - T_{H2O,in}) - (T_{CO2,in} - T_{H2O,out})}{ln\frac{(T_{CO2,out} - T_{H2O,in})}{(T_{CO2,in} - T_{H2O,out})}} \tag{3.5}$$

The total heat transfer coefficient is presented as a function of average bulk fluid temperature, T_b. The mean bulk temperature of CO_2 is calculated from an average of CO_2 inlet temperature and CO_2 outlet temperature, defined as:

$$T_b = \frac{T_{CO2,in} + T_{CO2,out}}{2} \tag{3.6}$$

In the experiments, the measured pressure drop in the gas cooler is the total pressure drop, which is calculated from the difference between inlet pressure and outlet pressure of fluid in the gas cooler. The measure pressure drop can be presented as:

$$\Delta P = P_{in} - P_{out} \tag{3.7}$$

The cold-side temperature approach is defined as the difference between CO_2 outlet temperature and water inlet temperature. This parameter is calculated based on the experimental data to evaluate the effectiveness of gas coolers. Here, the temperature approach can be presented as:

$$\Delta T_{approach} = T_{CO2,out} - T_{H2O,in} \tag{3.8}$$

4 Experimental results and discussion

Measurements are performed by systematically investigating the effects of different operating parameters (pressures, mass flow rates, and temperatures) on the pressure drops of both water and CO_2 sides, heat duty, supply temperature of SH and DHW circuits, overall heat transfer coefficient, and temperature approach difference. Table 4.1 presents the experimental results under the designed conditions in DHW mode, SH mode, and DHW+SH mode. The results obtained for SH gas cooler and two-pass DHW gas coolers are presented in detail in the following sections. The experimental results on the one-pass DHW gas coolers are summarized in Table 4.2.

Table 4.1: Experimental results under design condition.

parameter	Operation	DHW+SH	DHW+SH	SH	DHW	DHW
	Arrangement	2-pass	1-pass	1-pass	2-pass	1-pass
Pressure (bar)		85.48	85.53	85.35	100.34	99.84
Discharge temperature (°C)		80.36	81.63	80.13	95.48	94.17
DHW inlet temperature (°C)		13.07	11.54	-	10.95	10.64
SH inlet temperature (°C)		30.2	29.29	30.04	-	-
DHW mass flow rate (kg/min)		1.29	1.42	-	2.19	2.29
SH mass flow rate (kg/min)		11.54	11.72	23.1	-	-
CO_2 mass flow rate (kg/min)		2.41	2.43	2.49	2.1	2.18
DHW supply temperature (°C)		69.08	68.67	-	69.87	69.31
SH supply temperature (°C)		35.73	34.52	35.36	-	-
Pressure drop HX1,H_2O (bar)		0.058	2.46E-02	-	0.121	0.042
Pressure drop HX1,CO_2 (bar)		0.056	0.0769	-	0.031	0.056
Pressure drop HX2,H_2O (bar)		0.116	0.1208	0.408	-	-
Pressure drop HX2,CO_2 (bar)		0.003	0.0148	0.004	-	-
Pressure drop HX3,H_2O (bar)		0.159	0.0756	-	0.389	0.071
Pressure drop HX3,CO_2 (bar)		0.087	0.0004	-	0.076	0.063
Qaverage,HX1 (kW)		3.67	4.08	-	4.78	4.82
Qaverage,HX2 (kW)		4.48	4.37	8.5	-	-
Qaverage,HX3 (kW)		1.4	1.54	-	4.2	4.53
Temperature approach,HX1 (k)		14.17	14.56	-	8.32	8
Temperature approach,HX2 (k)		0.71	0.5	0.62	-	-
Temperature approach,HX3 (k)		7.79	6.52	-	8.24	7.96

Table 4.2: One-pass DHW gas cooler experimental results.

Pressure (bar)	Discharge temperature (°C)	DHW inlet temperature (°C)	SH inlet temperature (°C)	DHW mass flow rate (kg/min)	SH mass flow rate (kg/min)	CO_2 mass flow rate (kg/min)	Supply temperature (°C)	Pressure drop HX1,H_2O (bar)	Pressure drop HX1,CO_2 (bar)	Pressure drop HX3,H_2O (bar)	Pressure drop HX3,CO_2 (bar)
DHW operation											
100.8	98.7	10.9	-	2.3	-	2.2	71	-	-	-	-
101.3	96.2	11.1	-	2.3	-	2.2	70.7	0.094	0.057	0.077	0.065
99.8	94.2	10.6	-	2.3	-	2.2	69.3	0.042	0.056	0.071	0.063
100.1	95.1	10.7	-	2.5	-	2.1	66.3	0.035	0.045	0.114	0.048
100.2	94.2	10.5	-	2.4	-	2.2	68.8	0.164	0.057	0.115	0.063
99.9	94.4	10.8	-	2.3	-	2.2	69	-	-	-	-
99.8	95.2	10.6	-	2.3	-	2.2	69.2	0.059	0.052	0.072	0.059
100.2	94.5	10.5	-	2.4	-	2.2	68	-	-	-	-
95.5	100.5	12.6	-	2.1	-	2.1	72.2	0	0.057	0.086	0.082
92	94.3	11.1	-	1.8	-	3.3	81.8	0.04	0.125	0.099	0.28
100.2	100.4	19.9	-	1.8	-	3	86.5	0.014	0.101	0.039	0.212
90.2	93.7	20	-	1.8	-	3.1	79.9	0.004	0.113	0.004	0.256
96.1	100.5	13.7	-	1.5	-	2.5	85.3	0.048	0.083	0.051	0.152
91.5	95.9	15.5	-	2.1	-	3.8	82.1	0.025	0.151	0.067	0.374
90.2	95.5	17.5	-	2.9	-	3.3	70.9	0.019	0.115	0.108	0.227
94.2	94.6	11.1	-	2.1	-	2.4	71.8	0.063	0.073	0.111	0.115
93.8	95.2	11.2	-	2.1	-	2.3	71	0.063	0.069	0.12	0.101
97.4	98.6	14.6	-	2.3	-	2.3	72.5	0.061	0.066	0.115	0.096
96.9	98.7	11.7	-	2.1	-	2.9	78	0.066	0.09	0.125	0.166
98.2	98.6	14.9	-	2.3	-	2.7	75.5	0.07	0.081	0.131	0.132
97.5	94.5	10.6	-	2	-	2	70.8	0.055	0.055	0.059	0.068
95.2	90.9	11.8	-	2.1	-	2.5	71.4	0.029	0.072	0.132	0.123
95.4	94.3	11.8	-	2.1	-	2.3	71.5	0.031	0.069	0.134	0.098
97.2	94.6	13	-	2.2	-	2.1	70	0.027	0.058	0.146	0.075
97.1	95.4	13	-	2.1	-	2	69.6	0.022	0.055	0.15	0.066
96.6	96	15.8	-	2.2	-	2	68	0.016	0.055	0.147	0.059
97.3	94.6	14.9	-	2.2	-	2.1	69.5	0.018	0.058	0.146	0.068
96.8	94.2	13.9	-	2.2	-	2.1	69.2	0.012	0.057	0.125	0.07
97.4	97.2	14.1	-	2.1	-	2	69.6	0.017	0.054	0.135	0.062
96.9	97.7	13.7	-	2.1	-	1.9	69	0.011	0.05	0.129	0.055
98.6	100.2	13.4	-	2.1	-	1.8	68.3	0.024	0.041	0.13	0.043
91	92.7	11.5	-	1.9	-	2.2	70.2	0.001	0.067	0.102	0.095
94.5	96.5	10.6	-	1.4	-	2.3	81.4	0.005	0.077	0.093	0.118
DHW+SH operation											
85.5	81.6	11.5	29.3	1.4	11.7	2.4	68.7	0.025	0.077	0.076	0.0004
87.3	84.6	11.7	28.7	1.4	11.8	2.4	70.5	0.06	0.0004	0.081	0.057
89.3	89	11.3	26.4	1.4	11.9	2.2	72	0.038	0.063	0.065	0.051
79.4	68.1	11.2	29.5	1.9	12.3	3.4	59.6	0.022	0.132	0.107	0.329
79.3	73.9	11.2	29.6	1.9	13.9	3.1	61.6	0.114	0.113	0.095	0.283
80.2	73.5	15.5	33.9	2.1	11.7	3	60.1	0.098	0.107	0.112	0.15
81.7	79.8	11.2	32	1.6	12	2.8	66.8	0.009	0.1	0.11	0.093
83.8	83.7	16.9	31.1	2.1	12	2.7	63.7	0.134	0.082	0.113	0.082
84.3	82.5	13	36.2	2	10.3	2.8	66.2	0.019	0.094	0.109	0.126
84.4	87.4	13	36.1	2.2	10.2	2.9	66.3	0.012	0.098	0.117	0.127
85.5	84.8	13.1	31.8	1.9	13.1	3.2	69.3	0.131	0.108	0.114	0.114
84.1	82.2	13.1	35.6	1.9	11	3	67.3	0.125	0.105	0.136	0.105
86.2	88.4	16.8	35.8	2.1	10.6	2.8	68.4	0.137	0.092	0.134	0.092
85.1	83.2	16.4	35.9	2.1	10.7	3	67	0.138	0.103	0.134	0.105
81.9	79.2	16.3	34.6	2.1	10.6	3	63.7	0.027	0.105	0.131	0.107
79.3	78.5	16.3	33.1	2.1	10.8	2.9	61.6	0.015	0.103	0.121	0.142
79.4	74.7	11.8	33.1	2	10.9	2.8	59.8	0.039	0.099	0.121	0.134
81.4	83.1	11.9	33	2	10.8	2.3	61	0.029	0.076	0.125	0.068
81.5	77.5	13.2	29.1	2.1	13.1	2.7	59.8	0.054	0.084	0.131	0.074
86.5	74.2	18.9	32.4	1.8	12.6	3	64.1	0.052	0.094	0.156	0.026
85.8	71.5	15.3	33.8	1.7	12.6	3.3	64.7	0.124	0.115	0.057	0.146
86	70.9	14.1	36.5	2.1	11.1	3.2	61.3	0.062	0.113	0.102	0.156
86.3	71	13.8	34.9	2.1	11.4	2.9	59.9	0.058	0.093	0.087	0.116
86.4	69.7	11.7	35	1.5	12.1	2.9	63.3	0.034	0.104	0.106	0.114
86.2	73.7	13.7	32.2	1.2	12.3	2.1	64.5	0.058	0.066	0.075	0.051
86.5	83.5	12.9	33	1.2	12.3	2.2	71.4	0.032	0.073	0.094	0.0004
86.6	78	17.3	34.4	1.3	12.1	2.4	68.7	0.051	0.081	0.075	0.0004

4.1 Heat transfer coefficient

The total heat transfer coefficients are calculated based on the experimental data investigated under different operation conditions. Results obtained through this study are reported and discussed in this section.

4.1.1 Effect of CO_2-side pressure

To investigate the influence of gas cooler pressure on the total heat transfer coefficient, experimental studies are conducted. For a water inlet temperature of 13.1 °C, CO_2 mass flow rate of 2.15 kg/min, and discharge temperature of 97 °C, Figure 4.1 (a) presents the variations of the total heat transfer coefficients under the gas cooler pressures of 94 bar and 100 bar. As can be seen in this figure, with the increase of bulk mean temperature the heat transfer coefficient increases and then shows a downward trend, and there is a peak value in the variation of heat transfer coefficient. This is due to the dramatic changes in the thermophysical properties of CO_2 near the pseudo-critical temperature. The value of specific heat capacity reaches its maximum at the pseudo-critical temperature, which leads to the highest value of the heat transfer coefficient. In addition, the total heat transfer coefficient drops with an increase in the gas cooler pressure in the liquid-like region, and increasing the bulk temperature to a value higher than that of the pseudo-critical temperature results in a different trend. It is indicated that the heat transfer coefficient increases in the gas-like region due to different thermophysical properties of CO_2 under different pressures.

Figure 4.1 (b) presents the heat transfer coefficient with different gas cooler pressures under the test conditions of discharge temperature of 80 °C, DHW inlet water temperature of 21.8 °C, SH inlet water temperature of 30 °C, SH mass flow rate of 11.5 kg/min, and CO_2 mass flow rate of 2.4 kg/min, while the DHW mass flow rate varies between 1 kg/min and 2.5 kg/min. The CO_2 side bulk temperature decreases as the DHW mass flow rate increases from 1 kg/min to 2.5 kg/min. Furthermore, increasing the water-side mass flow rate increase the water-side heat transfer coefficient which can cause an increase in the total heat transfer coefficient. For each considered gas cooler operating pressure, heat transfer coefficients rise to a maximum value and then drops with decreasing CO_2 mean temperature. The heat transfer coefficients do not change significantly at high mean temperatures far from the pseudo-critical temperature (T_{SC}= 34.63 °C for P=80 bar and T_{SC}= 40 °C for P=90 bar). However, for bulk temperatures close to the pseudo-critical temperature, CO_2 thermodynamic properties including specific heat and thermal conductivity are significantly influenced by the operating pressure and mean temperature variations. Hence, in CO_2 working fluid, operating pressure has a considerable impact on the heat transfer coefficients in the near-critical region. This is because the specific heat and thermal conductivity go up significantly near the critical point region by decreasing operating pressure, therefore, the heat transfer coefficient tends to lift sharply in this region and the heat transfer is the best at the pseudo-critical point. For example, the specific heat capacity at 34.63 °C and 80 bar is 35.170 kJ/kg.K and at 40 °C and 90 bar is 12.833 kJ/kg.K. The variations of the thermophysical properties of CO_2 become higher when the operating pressure is closer to the critical pressure of CO_2. In addition, the peak point of the heat transfer coefficient shifts to the high-temperature state when the operating gas cooler pressure increases. This is because the pseudo-critical temperature shifts to the high-temperature region as the pressure increases.

4.1.2 Effect of CO_2-side mass flow rate

Figure 4.2 (a) shows the total heat transfer coefficient with different CO_2 mass flow rates under the condition of the gas cooler pressure of 100 bar, discharge temperature of 97 °C, and water inlet temperature of 13.1 °C. As shown in this figure, the heat transfer increases with increasing CO_2 mass flow rate, and this effect is more

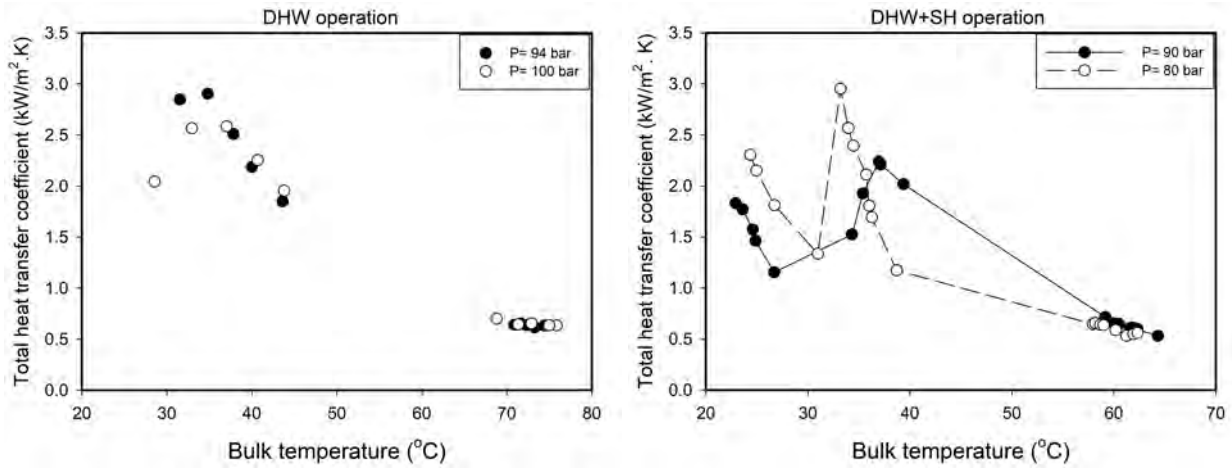

(a) **(b)**

Figure 4.1: Total heat transfer coefficient vs. bulk temperature for different pressures.

significant when the bulk mean temperature is near the pseudo-critical temperature. As the increase in the mass flow rate can result in a rise in the Reynolds number value, the diffusion rate also increases, and thus, the heat transfer coefficient enhances. Figure 4.2 (b) demonstrates the effect of CO_2 mass flow rate on the total heat transfer coefficient under the DHW+SH operation, considering the test conditions of 18 and 20 from Table 2.2. It is worth to note that the peak values of heat transfer coefficients under studied operating pressures occur at the temperatures slightly lower than the pseudo-critical temperature. Increasing the CO_2-side mass flow rate can enhance the total heat transfer coefficient. Specifically, the increase is more obvious at the region in the vicinity of the pseudo-critical point, where the total heat transfer coefficient undergoes a significant change and reaches a pick value. This indicates that the CO_2 mass flow rate has a great effect on heat transfer.

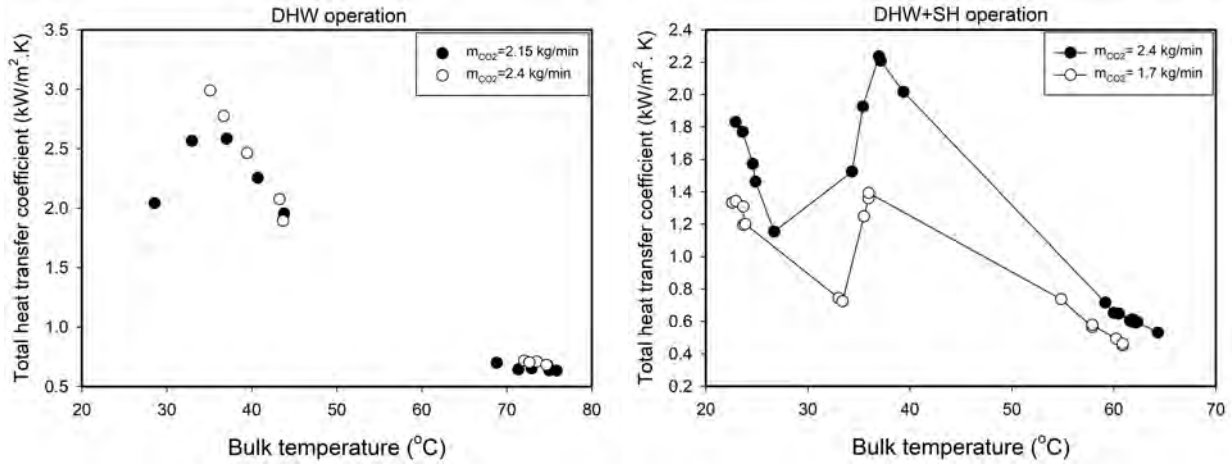

(a) **(b)**

Figure 4.2: Total heat transfer coefficient vs. bulk temperature for different CO_2 mass flow rates.

4.1.3 Effect of H_2O-side temperature

The experimental heat transfer coefficients with water inlet temperatures under the condition of gas cooler pressure of 94 bar, discharge temperature of 97 °C, and CO_2 mass flow rate of 2.15 kg/min are presented in Figure 4.3 (a). As shown, no significant and clear influence of the water inlet temperature is demonstrated on the heat transfer coefficients when CO_2 is in a high-temperature state. The effect of DHW water inlet temperature on the total heat transfer coefficient under DHW+SH operation is depicted in Figure 4.3 (b). The increase of temperature from 12.8 °C to 17.8 °C has a minor effect on the heat transfer coefficient in the high-temperature state. However, the higher the DHW water inlet temperature, the higher the total heat transfer coefficient in the liquid-like region.

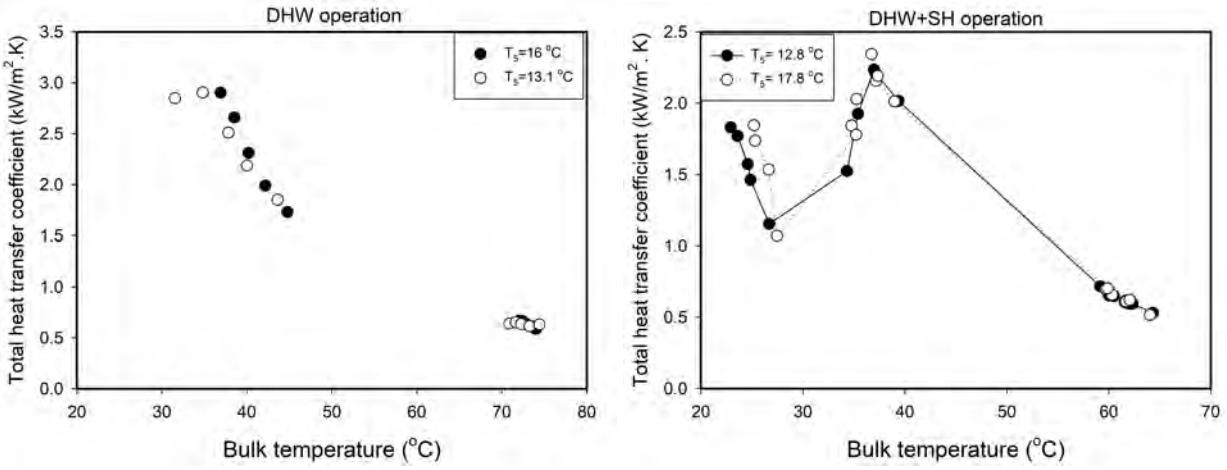

Figure 4.3: Total heat transfer coefficient vs. bulk temperature for different water inlet temperatures.

4.2 Heat Duty

The capacity for each of the data points obtained under different conditions is presented in this section. The influence parameters include the CO_2-side pressure, CO_2-side mass flow rate, H_2O-side mass flow rate, and H_2O-side temperature. For the counter-flow gas coolers, the energy difference between the water side and refrigerant side is calculated, and the maximum relative deviation is less than 5%. Taking DHW operation as an example, it is found that there is an energy balance between the water and CO_2, as presented in Figure 4.4. The average heat duty is defined, and the results are presented in the following subsections.

4.2.1 Effect of CO_2-side pressure

Figure 4.5 (a) presents the average heat duties at the water inlet temperature of 13.1 °C, CO_2 mass flow rate of 2.15 kg/min, and discharge temperature of 97 °C for the gas cooler pressures of 94 bar and 100 bar under DHW operation. As can be seen from this figure, increasing the DHW mass flow rate leads to an increase in the average heat duty of DHW operation. In addition, the increase in the pressure from 94 bar to 100 bar causes the values of heat duty in the gas cooler go up in the lower DHW mass flow rates. Figure 4.5 (b) indicates the effects of DHW mass flow rate and operating CO_2 pressure on heat duty under DHW+SH operation. For all data, a higher water mass flow rate yields a higher heat duty. This indicates that the heat duty of DHW gas cooler under DHW+SH operation with different pressure is linearly proportional to the mass flow rate. The pressure effect is more pronounced at

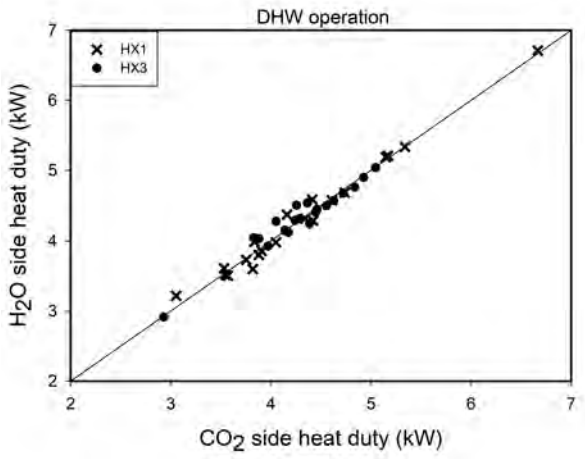

Figure 4.4: Heat duties in the CO_2 side vs. H_2O side in the preheating and reheating gas coolers.

higher water mass flow rates. However, for the experimental conditions in this study, increasing the pressure from 80 bar to 90 bar results in a different trend in the SH gas cooler under DHW+SH operation (Figure 4.5 (c)).

4.2.2 Effect of CO_2-side mass flow rate

The experimental average heat duties with respect to the variations of the DHW mass flow rate are shown in Figure 4.6. Figure 4.6 (a) presents the results under the gas cooler pressure of 100 bar, discharge temperature of 97 °C, and water inlet temperature of 13.1 °C. Figure 4.6 (a) presents the experimental results under the test conditions of 18 and 20 from Table 2.2. The effect of the CO_2 mass flow rate is more significant in higher DHW mass flow rates. A higher CO_2 mass flow rates leads to a higher heat duty under both DHW and DHW+SH operations. As an example, consider the data points with a DHW mass flow rate of approximately 1.77 kg/min in Figure 4.6 (a). Increasing the CO_2 mass flow rate from 2.15 kg/min to 2.4 kg/min yields values of heat duty of 7.83 kW and 8.02 kW, respectively. Contrast this for data points with a DHW mass flow rate of nearly 2.58 kg/min, where the same increases in CO_2 mass flow rate yield the heat duties that are 9.61 kW and 10.21 kW, respectively. The effects of CO_2 and SH mass flow rates on the SH gas cooler heat duty are shown in Figure 4.7. A clear trend of increasing heat duty with increasing mass flow rates is demonstrated for all recorded data. At a given operating CO_2-side pressure, increasing water mass flow rate can enhance the heat duty. This is attributed to the higher water-side heat transfer in the gas cooler due to a higher value of mass flow rate, thereby resulting in a higher heat duty. For these investigated data points, it is found that SH mass flow rate is relatively less important, and the effect of increased CO_2 mass flow rate is somewhat higher on the heat duties.

4.2.3 Effect of H_2O-side temperature

The average heat duty is plotted as a function of the water mass flow rate in Figure 4.8 under DHW, SH, and DHW+SH operations. The measured heating capacity ranges from nearly 3.5 kW to 9.7 kW depending on the test conditions and operating mode. As the water inlet temperature increases, the water outlet temperature tends to increase. It can be seen from Figure 4.8 that as the water inlet temperature increases, the average heat duty decreases due to lower temperature difference. The influence of water mass flow rate dominates the inlet temperature for the DHW loop, and the heat duty increase linearly as the mass flow rate increases. With the decrease of the mass flow rate of water, both the water and CO_2 outlet temperatures demonstrate increasing trends while the heat capacity

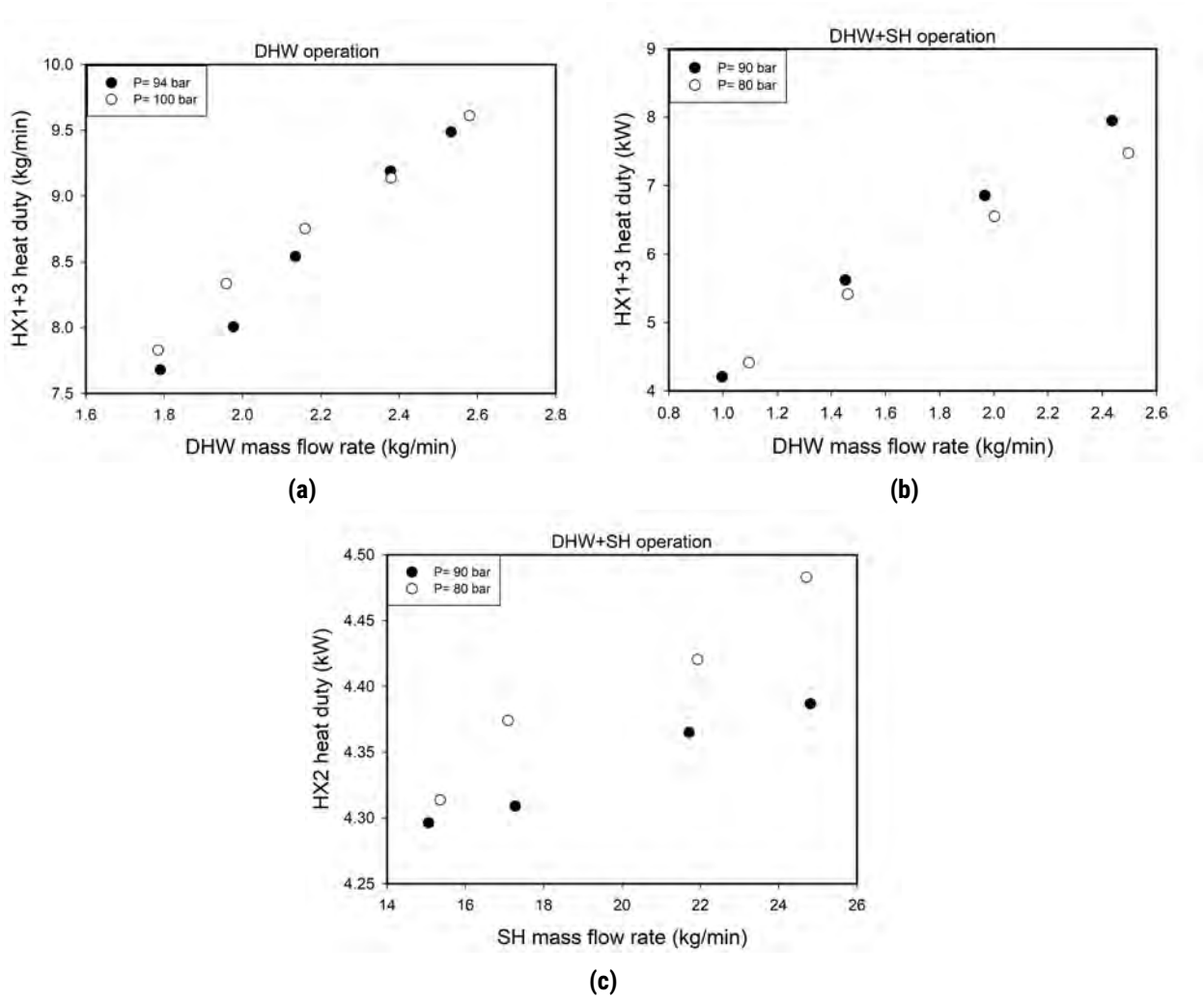

Figure 4.5: Heat duty vs. water mass flow rate for different pressures in (a) DHW operation and (b,c) DHW+SH operation.

decreases. As a result, the higher outlet temperature of CO_2 causes the heat capacity to become low which results in a drop in the cycle performance. It can be concluded that the lower inlet temperature of water at an optimum water mass flow rate can help to increase the heat duty of gas cooler under different operation modes.

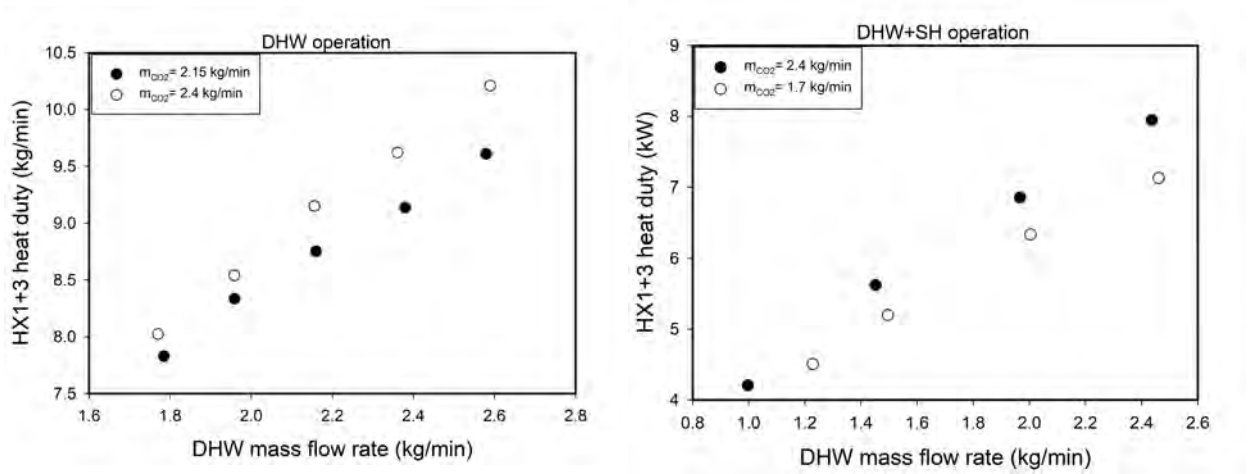

Figure 4.6: Heat duty vs. DHW mass flow rate for different CO_2 mass flow rates in (a) DHW operation and (b) DHW+SH operation.

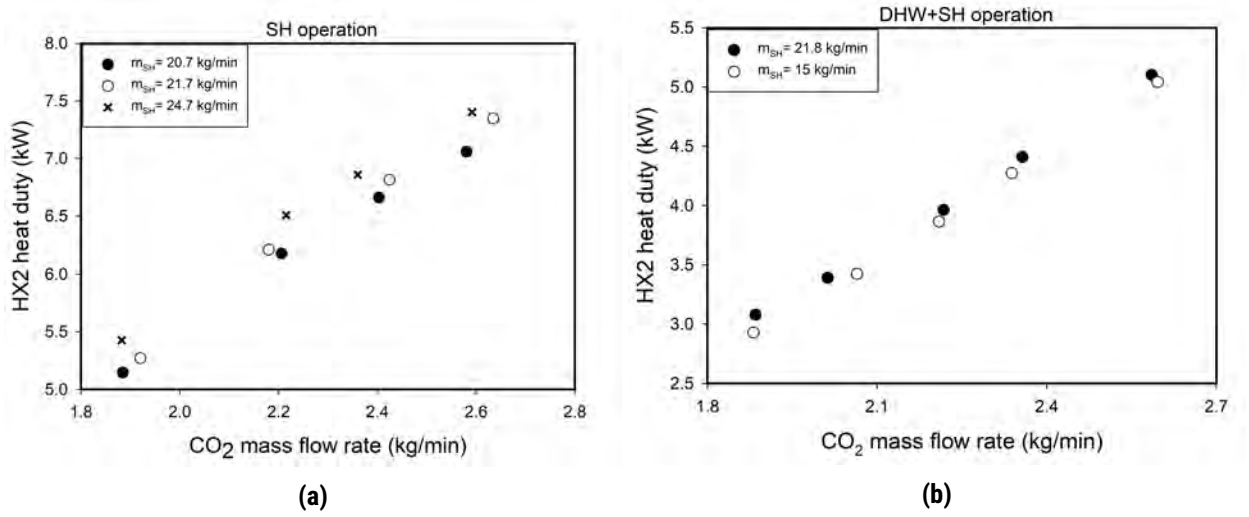

Figure 4.7: Heat duty vs. CO_2 mass flow rate for different SH mass flow rates in (a) SH operation and (b) DHW+SH operation.

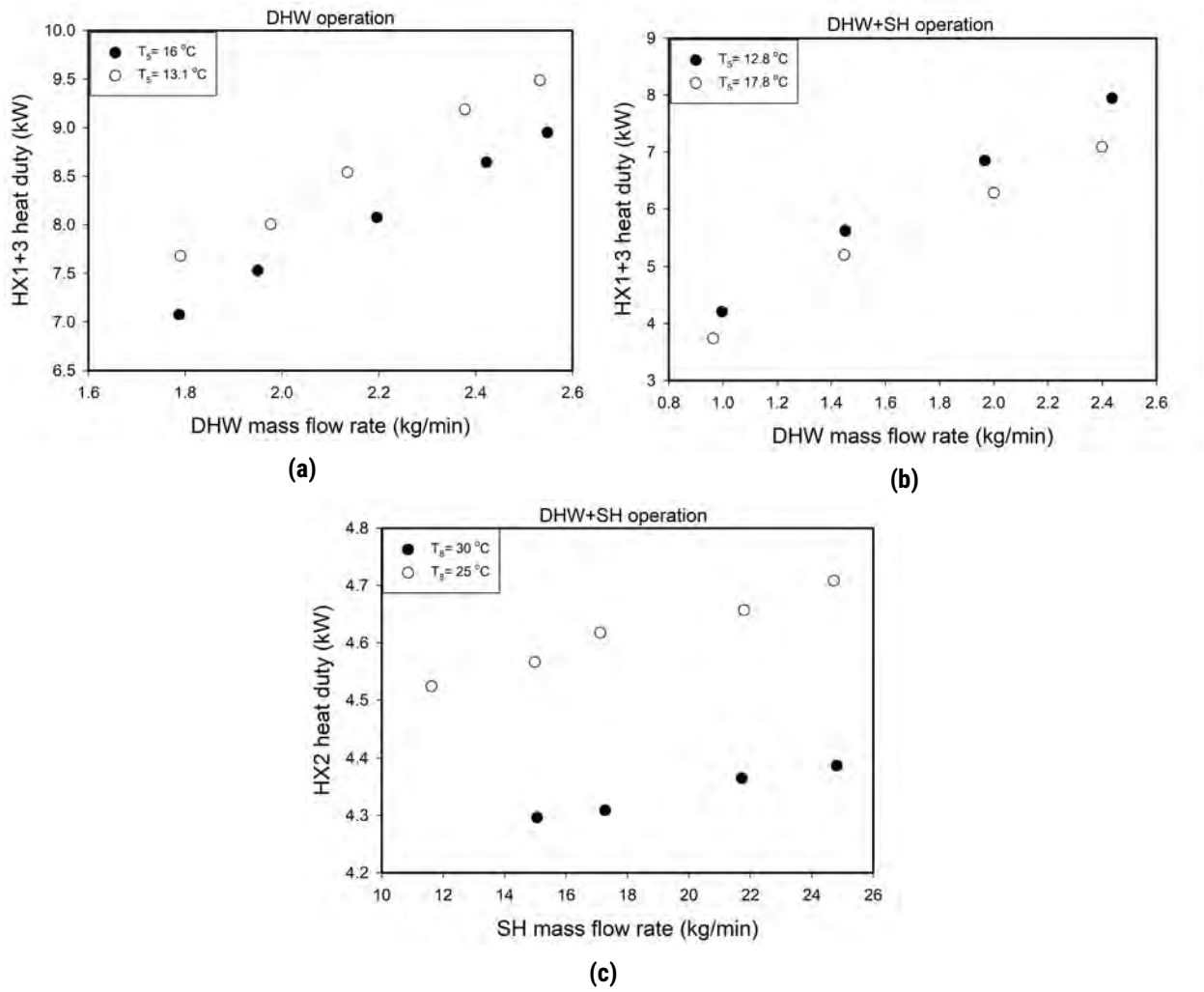

Figure 4.8: Heat duty vs. water mass flow rate for different water inlet temperatures in (a) DHW operation and (b,c) DHW+SH operation.

4.3 Pressure drop

The pressure drops are measured and recorded for each data sample. In this section, the influence of different important operating parameters on the pressure drop is presented.

4.3.1 Effect of CO_2-side pressure

Figure 4.9 gives the pressure drop distribution as a function of the bulk temperature under the condition of water inlet temperature of 13.1 °C, CO_2 mass flow rate of 2.15 kg/min, and discharge temperature of 97 °C at gas cooler pressures of 94 bar and 100 bar. The pressure drop increases as the bulk temperature increases due to a decrease in the average density which leads to an increase in the average velocity of the cross-section. It can be seen that at a given temperature, as the gas cooler pressure increases, the pressure drop decreases. The increase in the hot side fluid pressure can cause an increase in the density and thus a decrease in the velocity of CO_2, so the pressure

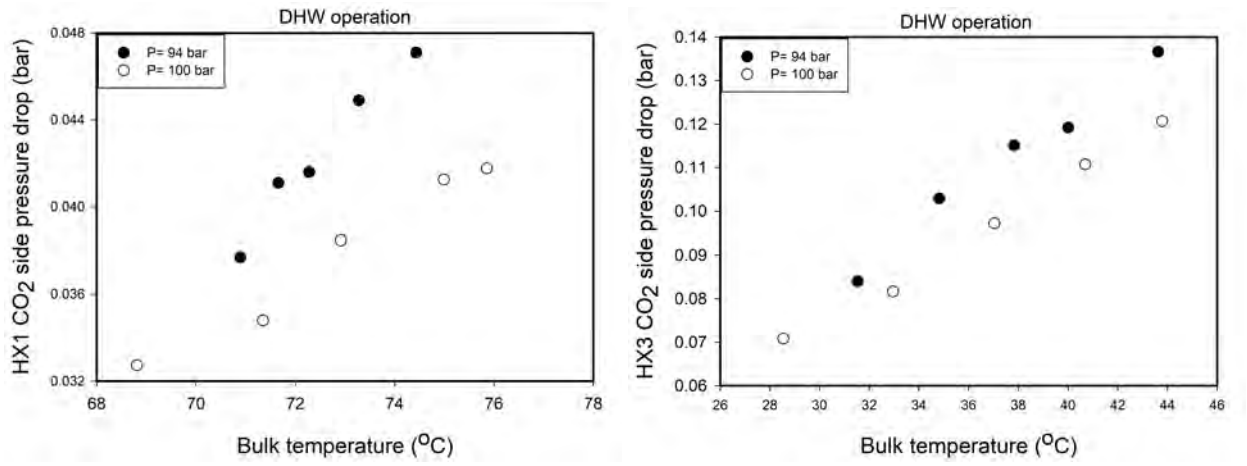

Figure 4.9: Pressure drop vs. bulk temperature for different pressures in DHW operation.

drop decreases. The pressure drop is slightly influenced by the inlet pressure when the bulk temperature is lower than the pseudo-critical temperature (T_{SC}= 42 °C for P=94 bar and T_{SC}= 45 °C for P=100 bar), Figure 4.9 (b). The values of pressure drop sharply rise with decreasing gas cooler pressure at the bulk temperatures higher than that of the pseudo-critical temperature (Figure 4.9 (a)).

Figure 4.10 (a)-(c) indicates the effects of gas cooler pressure and water mass flow rate on the water-side pressure drop of the tri-partite gas cooler in the DHW+SH operation. The experiments under DHW section (Figure 4.10 (a),(c),(d),(f)) are performed with a discharge temperature of 80 °C, DHW inlet temperature of 12.8 °C, SH water inlet temperature of 30 °C, SH mass flow rate of 11.5 kg/min, and CO_2 mass flow rate of 2.4 kg/min. To monitor the performance of SH section (Figure 4.10 (b),(e)), the experiments are carried out at the above operating conditions while keeping DHW mass flow rate at 1.3 kg/min and varying the SH mass flow rate between 15 kg/min and 24.8 kg/min. The water-side pressure drop increases sharply with the increase in the water mass flow rate. A higher mass flow rate thickens the film thickness and enhances the velocity, which leads to a higher pressure drop. The influence of gas cooler pressure on the water-side pressure drops of space heating and preheating gas coolers is negligible under the studied cases, but becomes noticeable on the reheating gas cooler. In general, the influence of water mass flow rate on the pressure drop of the water-side dominates the gas cooler pressure in the three gas coolers. The water-side pressure drop in the reheating gas cooler in lower than the preheating gas cooler. It is attributed to the viscosity. Unlike the DHW operation, increasing the gas cooler pressure from 80 bar to 90 bar in DHW+SH results in a different trend. In the DHW+SH operating mode, the water outlet of the preheating gas cooler is higher at 80 bar; therefore, the water-side pressure drop in the preheating gas cooler increases as the gas cooler pressure increases. Figure 4.10 (d)-(f) shows the variation in the CO_2-side pressure drop between the inlet and the outlet of the gas coolers with the bulk mean temperature of CO_2 for two different operating pressures, 80 bar and 90 bar. The pressure drop reduces with the operating gas cooler pressure because the variation in the thermodynamic properties becomes lower as the operating gas cooler pressure rises. As shown, when the bulk mean temperature is less than the pseudo-critical temperature (T_{SC}= 34.63 °C for P=80 bar and T_{SC}= 40 °C for P=90 bar), the CO_2-side pressure drop increases gradually with the increase of gas cooler pressure (Figure 4.10 (f)), and the effect of operating pressure is more significant when the bulk mean temperature is near the pseudo-critical.

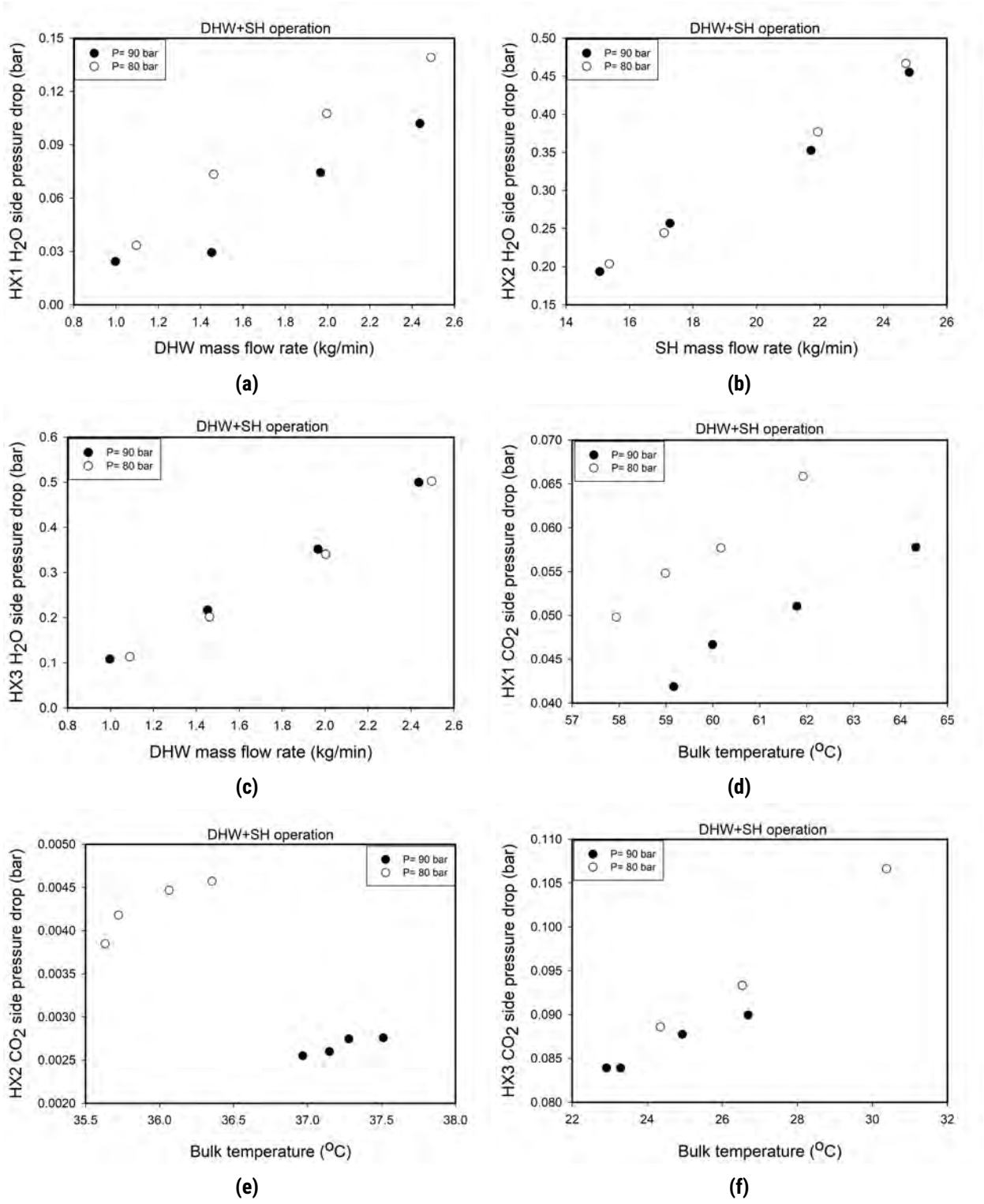

Figure 4.10: Pressure drop vs. (a-c) DHW mass flow rate and (d-f) bulk temperature for different pressures in DHW+SH operation.

4.3.2 Effect of CO_2-side mass flow rate

Figure 4.11 shows the measured pressure drops for mass flow rates of 2.15 kg/min and 2.4 kg/min at a water inlet temperature of 13.1 °C, discharge temperature of 97 °C, and gas cooler pressure of 100 bar. The pressure drop increases as the CO_2 mass flow rate increases at different bulk temperatures due to a rise in the Reynolds number. In particular, for the reheating gas cooler with a bulk temperature of approximately 72.7 °C, the measured pressure drop is 0.038 bar for a mass flow rate of 2.15 kg/min and 0.046 bar for a mass flow rate of 2.4 kg/min. As mentioned above, the pressure drop rises with increasing the bulk temperature. The higher average refrigerant temperature results in a lower average density and higher average velocity through the gas cooler, resulting in a higher pressure drop. At the mass flow rate of 2.15 kg/min, the pressure drop in the preheating gas cooler increases from 0.071 bar to 0.13 bar when the bulk temperature rises from 28.5 °C to 43.8 °C (i.e., the percentage of growth is 81% for a temperature change of 15.3 °C).

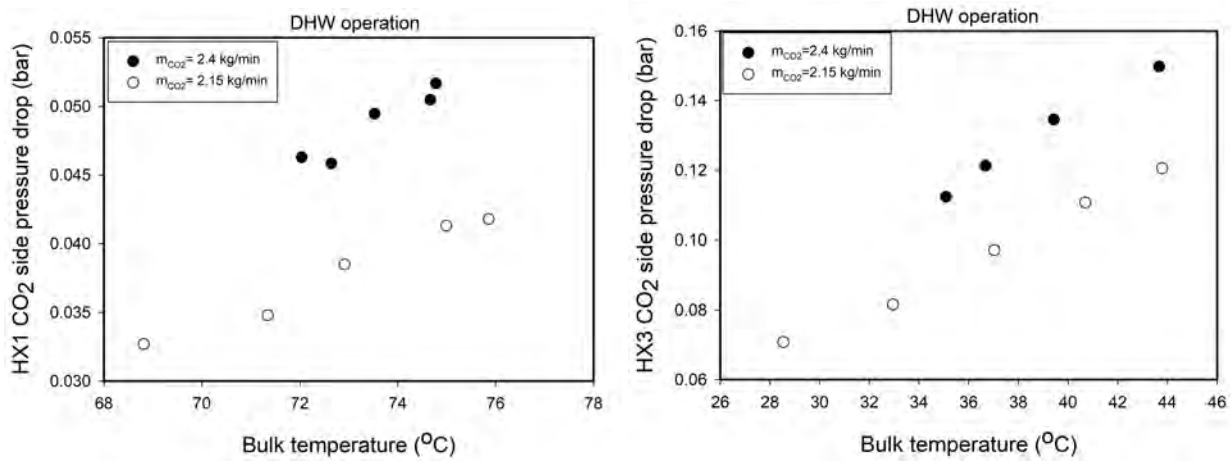

Figure 4.11: CO_2 side pressure drop vs. bulk temperature for different CO_2 mass flow rates in DHW operation.

Figure 4.12 (a) and (b) shows the variation of CO_2-side pressure drop with varying CO_2 mass flow rates in the gas coolers. The mass flow rate of SH is maintained at 24.8 kg/min in Figure 4.12 (a) and at 21.8 kg/min and 15 kg/min in Figure 4.12 (b) with constantly keeping the gas cooler pressure of 85 bar, discharge temperature of 80 °C, DHW water inlet temperature of 12.6 °C, SH water inlet temperature of 30 °C, and DHW mass flow rate of 1.3 kg/min. Test results demonstrate that the pressure drop of CO_2 side increases from 0.038 bar to 0.11 bar for the reheating and preheating gas coolers and from 0.002 bar to 0.004 bar for the space heating gas cooler while the CO_2 mass flow rate increases from 1.8 kg/min to 2.6 kg/min. The maximum pressure drops for the reheating, space heating, and preheating heat exchangers are 0.65 bar, 0.11 bar, and 0.004 bar at nearly the mass flow rate of 2.6 kg/min, respectively. The CO_2-side pressure drop of SH gas cooler increases slightly as the mass flow of the water side decreases. The experimental results show that the slop of CO_2 side pressure drop in the preheating gas cooler changes sharper than the reheating gas cooler at the high CO_2 mass flow rate. As expected, the CO_2 mass flow rate has a significant influence on the CO_2 side pressure drop, the pressure drop rises with a higher mass flow rate at a fixed operating gas cooler pressure. This is because the higher bulk temperature can result in a higher average velocity of flow and Reynolds number.

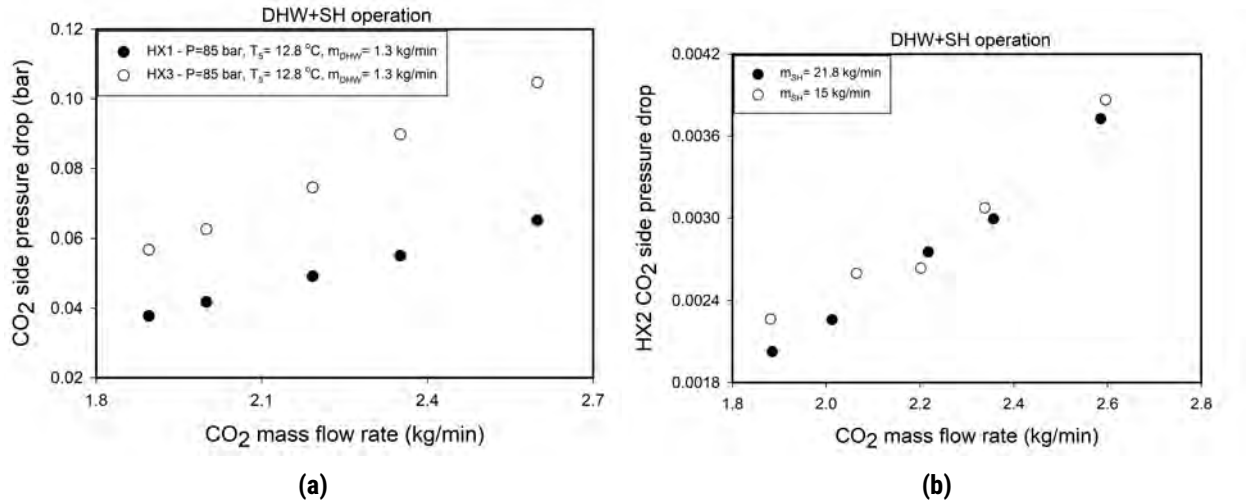

Figure 4.12: Pressure drop vs. CO_2 mass flow rate in DHW+SH operation.

4.3.3 Effect of H_2O-side temperature

Figure 4.13 gives the influence of different DHW mass flow rates on the water-side pressure drop at CO_2 mass flow rate of 2.15 kg/min, discharge temperature of 97 °C, and gas cooler pressure of 94 bar for the inlet temperature of 16 °C and 13.1 °C. An increase in the DHW mass flow rate causes an increase in the pressure drop at constant gas cooler pressure. When DHW mass flow rate increases from approximately 1.8 kg/min to 2 kg/min at a water inlet temperature of 16 °C, the water-side pressure drop increases sharply from almost 0.01 bar to 0.06 bar and 0.04 bar to 0.27 bar for the reheating and preheating heat exchangers, respectively. At the same time, it can be seen from the figure that at a given mass flow rate and gas cooler pressure, the water-side pressure drop increases with decreasing water inlet temperature, since as the inlet temperature increases, the viscosity decreases. The influence of water inlet temperature on the pressure drop is more obvious at the DHW mass flow rate of 1.8 kg/min. The variations in the pressure drop with the bulk mean temperature at the CO_2 mass flow rate of 2.15 kg/min, discharge temperature of 97 °C, and gas cooler pressure of 94 bar are compared in Figure 4.13 (c) and (d) for two different water inlet temperatures of 16 °C and 13.1 °C. The increase of CO_2 mean temperature flowing through the gas coolers causes a decrease in the density and viscosity of the refrigerant to maintain the flow continuity, resulting in a larger Reynolds number and pressure drop.

Figure 4.14 demonstrates the effect of SH mass flow rate on the water-side pressure drop of the space heating gas cooler under three different SH water inlet temperatures in SH operating mode. The gas cooler pressure is maintained at 90 bar for a given discharge temperature of 76 °C, and CO_2 mass flow rate of 2.4 kg/min. It is found that the pressure drop of water side increases from 0.32 bar to 0.46 bar when the SH mass flow rate varies from 20.6 kg/min to 24.8 kg/min, and the pressure drop increases with decreasing the operating water inlet temperature. The trend lines with the variation of temperature are similar under the same operating condition. The pressure drop is less affected by the water inlet temperature, while the mass flow rate of water has a significant influence on the pressure drop. In the space heating gas cooler, the pressure drop at 25 °C produces 0.0187 bar and 0.0218 bar higher than those of 35 °C for the SH mass flow rates of 20.6 kg/min and 24.8 kg/min, respectively.

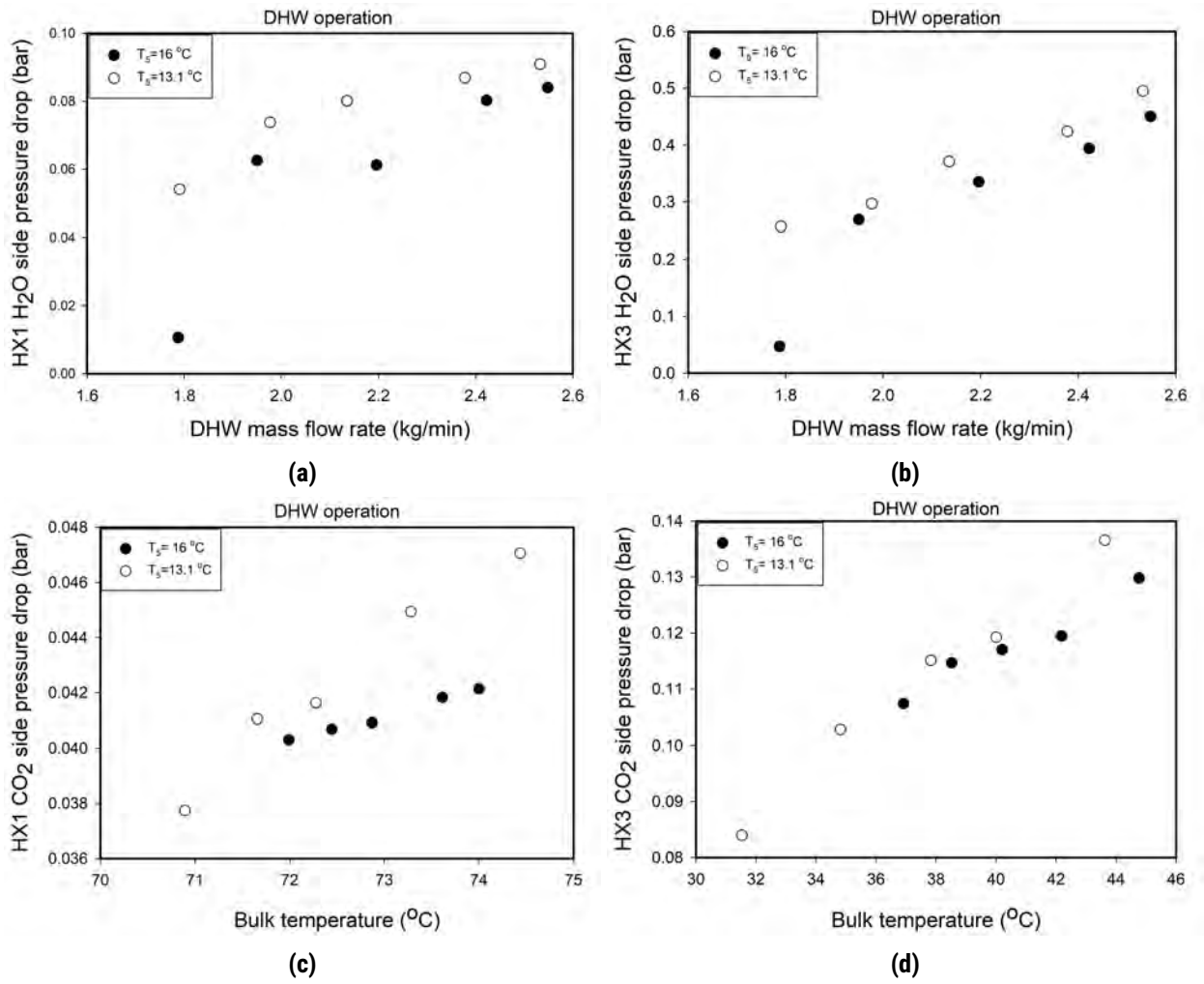

Figure 4.13: The effect of water-side temperature on (a,b) water-side pressure drop and (c,d) CO_2-side pressure drop in DHW operation.

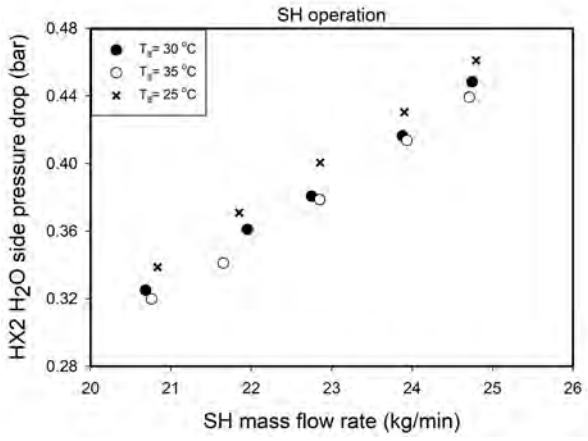

Figure 4.14: The effect of water-side temperature on water-side pressure drop in SH operation.

4.4 Supply temperature

The supply temperature is measured for each point following the procedures described in Section 2. In this section, the results and trends are presented, and the influences of different parameters are discussed.

4.4.1 Effect of CO_2-side pressure

Figure 4.15 (a) shows the experimental results of the DHW supply temperature. For experiments carried out in the study, the DHW mass flow rate is varying from 1.8 kg/min to 2.6 kg/min. In general, the outlet temperature of the water side is higher than that obtained at the CO_2 side due to the counter-flow arrangement in the gas coolers under study. A comparison between the experimental results obtained under different evaluated cases indicates that the outlet temperatures decrease linearly as the mass flow rate of the water side increases. At a constant water inlet temperature of 13.1 °C, CO_2 mass flow rate of 2.15 kg/min, and discharge temperature of 97 °C, for the case with the variation of gas cooler pressure, a relationship between the DHW outlet temperature and the mass flow rate of the water side is shown in Figure 4.15 (a). The outlet temperature of water increases as the gas cooler pressure increases. The same behavior is observed in Figure 4.15 (a) under DHW+SH where the experiments are conducted under the conditions of 18 and 21 from Table 2.2. The influence of pressure on the outlet temperature is more significant in the lower and higher DHW mass flow rates under DHW and DHW+SH operation, respectively. The SH supply temperature versus mass flow rates for SH operation and DHW+SH operation are shown in Figure 4.15 (b). For the SH loop, the experiments are conducted under the test conditions of 5 and 6 under SH operation and the test conditions of 14 and 16 under DHW+SH operation from Table 2.2. In contrast to DHW operation, an increase in operating pressure leads to a lower value of SH supply temperature under SH operation. This trend in the SH supply temperature is also found when the system is operated under the DHW+SH operation.

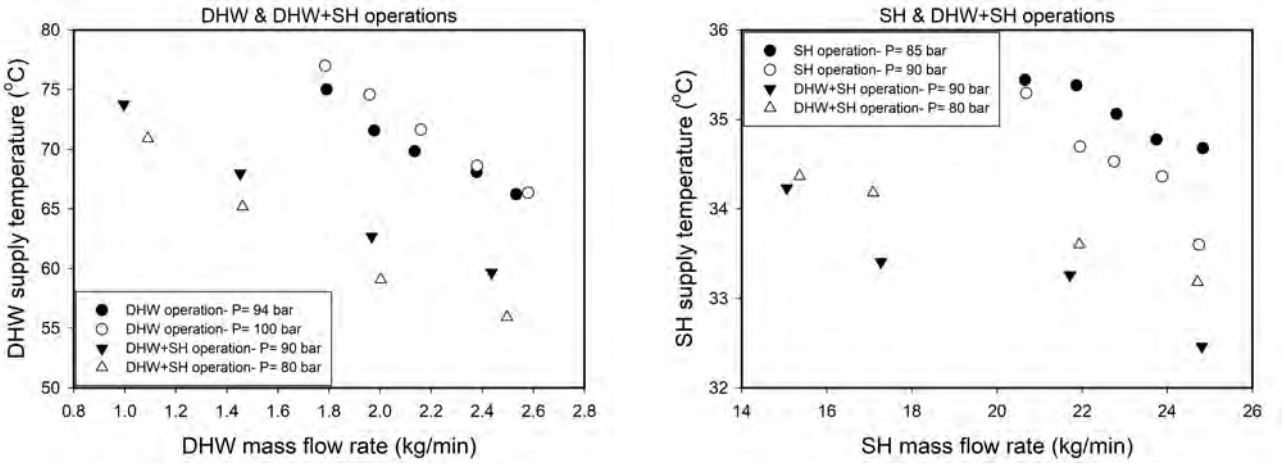

(a) **(b)**

Figure 4.15: Supply temperature vs. water mass flow rate for different gas cooler pressures.

4.4.2 Effect of CO_2-side mass flow rate

Figure 4.16 shows the effects of CO_2 and DHW mass flow rates on the supply temperature under three different operating modes.

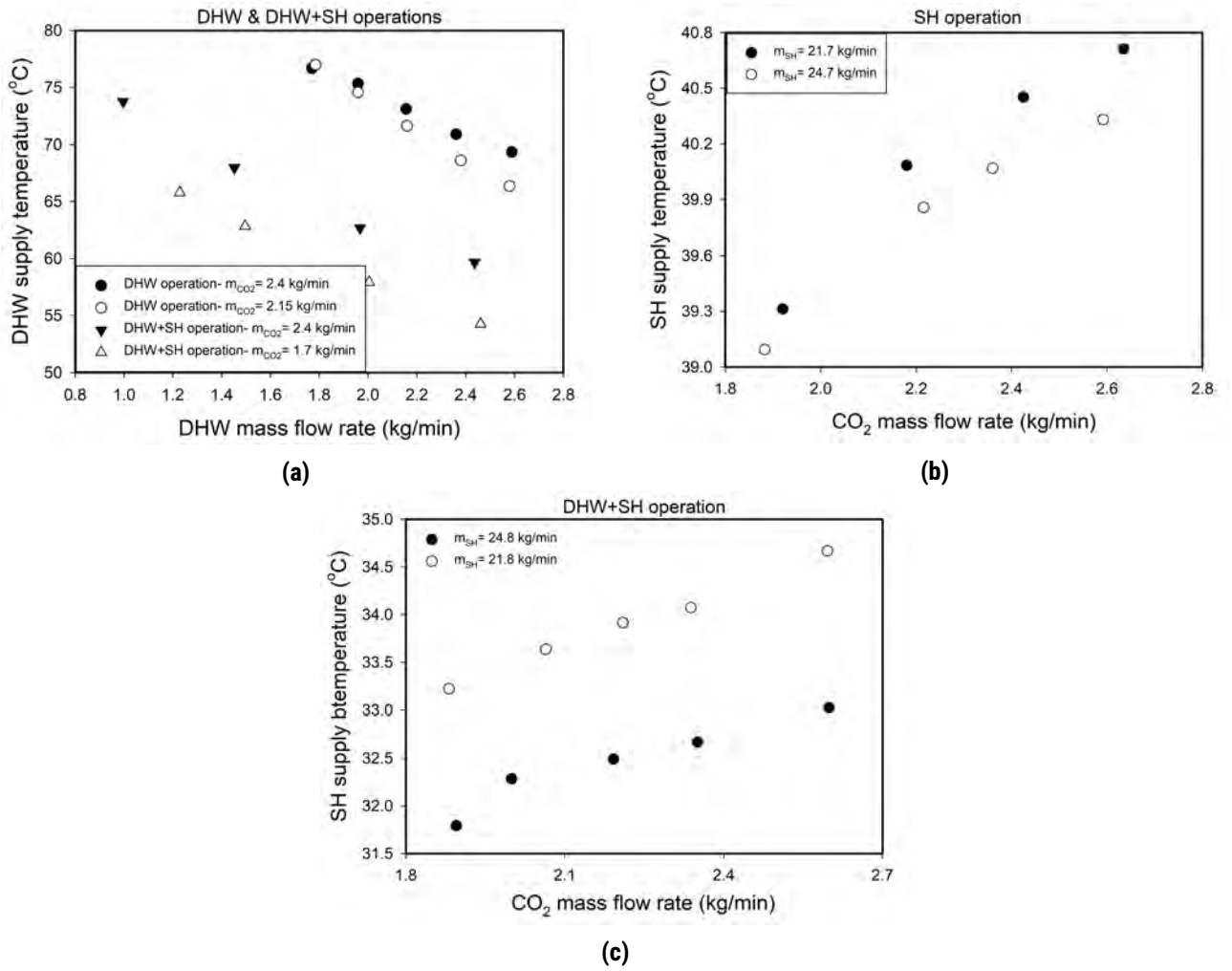

Figure 4.16: Supply temperature vs. (a) DHW mass flow rate for different CO_2 mass flow rates and vs. (b,c) CO_2 mass flow rate for different SH mass flow rates.

According to the results, a larger mass flow rate of refrigerant and a lower water mass flow rate increase the water outlet temperature. On one hand, the flow velocity of water declines due to the decrease of water mass flow rate, thereby resulting in a lower heat transfer in the water side of the gas coolers. Hence, the lower the water mass flow rate, the higher the water outlet temperature, which can lead to a lower heat duty. So, the water mass flow rates through the gas coolers need to be properly selected and controlled to provide the hot water temperature of above 70 °C and SH temperature of above 35 °C. On the other hand, at a given operating gas cooler pressure, the supply temperature is directly affected by the CO_2 inlet temperature as the gas coolers are designed to work in a counter-flow configuration. Therefore, at a fixed pressure, an increase in the water mass flow rate leads to a decline in the water outlet temperature. It is found that the DHW outlet temperatures of m_{CO_2}=2.4 kg/min are higher than those of m_{CO_2}=2.15 kg/min, as shown in Figure 4.16 (a). Figure 4.16, in general, indicates that the outlet temperatures decrease linearly as the mass flow rate of the water side increases. In addition, lower CO_2 mass flow rate leads to a lower supply temperature. For the gas cooler with m_{CO_2}=2.4 kg/min, a DHW outlet temperature of almost 71 °C is achieved at DHW mass flow rate of 2.4 kg/min having a fixed gas cooler pressure of 100 bar, discharge temperature of 97 °C, and water inlet temperature of 13.1 °C, while a lower DHW mass flow rate is required to achieve the same

outlet temperature of water at the lower CO_2 mass flow rate (Figure 4.16 (a)). It is found that when the water mass flow rate is decreased to get a higher water outlet temperature, a decrease of the heat transfer coefficient of the water side also occurs. Adjustment of the water mass flow rate is one of the critical ways to get different supply water temperatures at the outlet of the gas cooler.

4.4.3 Effect of H_2O-side temperature

It is shown from Figure 4.17 (a) that under DHW operation at specified CO_2 mass flow rate of 2.15 kg/min, discharge temperature of 97 °C, and gas cooler pressure of 94 bar the DHW supply temperature is higher at higher water inlet temperature and the water temperature lift varies from nearly 53 °C to 61°C and 51 °C to 58 °C at the water inlet temperatures of 13.1 °C and 16 °C, respectively. The trend lines for supply temperature under different conditions in SH and DHW+SH operations are similar. This is because as the water inlet temperature increases, the CO_2 outlet temperature increases, thereby the water outlet temperature is higher, as seen in Figure 4.18. This mechanism influences also on the gas cooler outlet enthalpy status. Under the test conditions of Figure 4.17 (a) in DHW operation, the CO_2 outlet temperature of the gas cooler increases from 27.3 °C to 36.8 °C and from 19.4 °C to 35.4 °C when the water inlet temperatures are 16 °C and 13.1 °C, respectively. When the supply temperatures are 68.8 °C (T5=16 °C and m_{DHW}=2.4 kg/min) and 69.8 °C (T5=13.1 °C and m_{DHW}=2.15 kg/min), the CO_2 outlet temperature of gas cooler is higher than the critical temperature (T_c=31.1 °C). This indicates that CO_2 liquid phase enters the throttling device when up to this condition. However, when the outlet temperature increases, supercritical CO_2 enters the throttling device. Lower CO_2 outlet temperature is desired to increase the system performance. Therefore, one solution is to cool down the CO_2 high temperature using an internal heat exchanger before entering the throttling device.

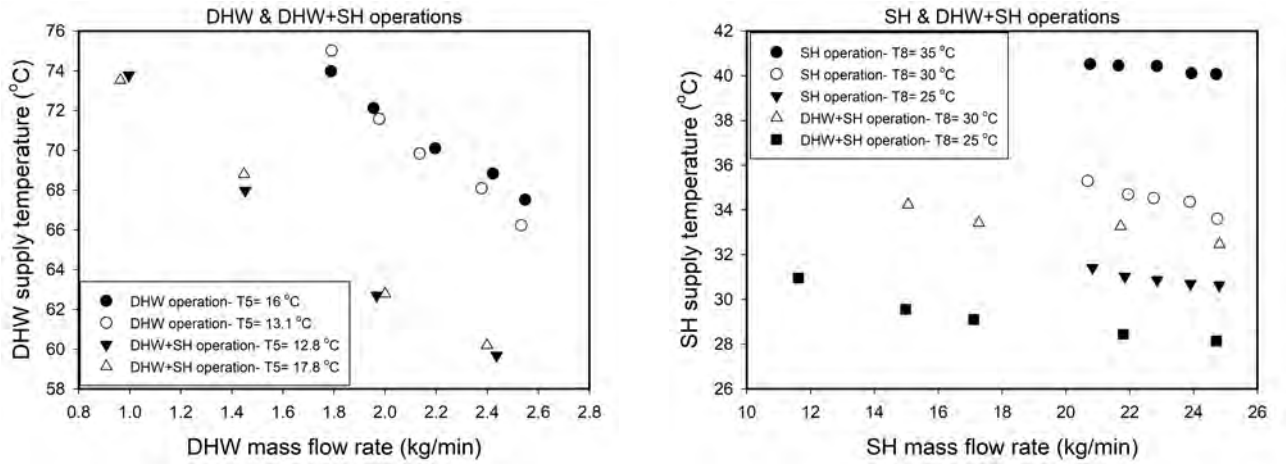

(a) **(b)**

Figure 4.17: Supply temperature vs. water mass flow rate for different water inlet temperatures.

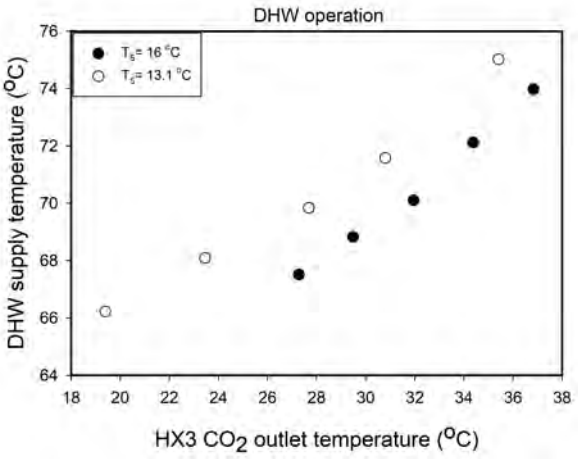

Figure 4.18: DHW supply temperature variation vs. GC3 CO_2 outlet temperature for different water inlet temperatures.

4.5 Temperature approach

Temperature approach is an important parameter to evaluate the effectiveness of considered heat exchangers under different conditions. A lower value of temperature approach in the heat exchangers presents the heat exchangers are appropriately sized and selected for the operating conditions, resulting in a lower enthalpy at the inlet of evaporator and the higher system performance. The influences of DHW mass flow rate, gas cooler pressure, water inlet temperature, and CO_2 mass flow rate on the temperature approach for both preheating and reheating gas coolers are shown in Figure 4.19.

Figure 4.19 (a) indicates that increasing the DHW mass flow rate can enhance the value of temperature approach. Specifically, the increase is more obvious at higher mass flow rates, but slightly increase when the DHW mass flow rate is small. It can also be found that the contribution of CO_2 mass flow rate to the temperature approach is higher when the DHW mass flow rate is high, but becomes smaller as the DHW mass flow rate keeps decreasing. At constant pressure and water mass flow rate, a higher CO_2 mass flow rate and water inlet temperature decreases the temperature approach in the reheating gas cooler while leads to an increase in its value in preheating gas cooler under DHW operation. The temperature approach of reheating gas cooler varies between nearly 4.5 °C and 11.5 °C, depending on the operating condition. Under the same operating conditions, Figure 4.19 (b) indicates the experimental results of the preheating gas cooler temperature approach. Evaluation of Figure 4.19 (b) for the preheating gas cooler presents an opposite trend than that of the reheating gas cooler. A lower value of temperature approach indicates that the gas cooler is sized well. In general, this gas cooler is associated with much higher temperature approaches than those of the reheating gas cooler, indicating that it is undersized for almost all evaluated cases at the low DHW mass flow rate in DHW operation. A higher heat transfer area is required to lower the value of the temperature approach . For the gas cooler pressure of 100 bar, water inlet temperature of 13.1 °C, CO_2 mass flow rate of 2.4 kg/min, and DHW mass flow rate of 1.8 kg/min, the temperature approach is as high as 22 °C, which comes down to lower than 4 °C when the DHW mass flow rate increases to 2.6 kg/min and CO_2 mass flow rate drops to 2.15 kg/min.

Figure 4.19 (c) and (d) shows the temperature approach of the reheating and preheating gas coolers in DHW+SH operation under different operating conditions. For the SH water inlet temperature of 30 °C and SH mass flow

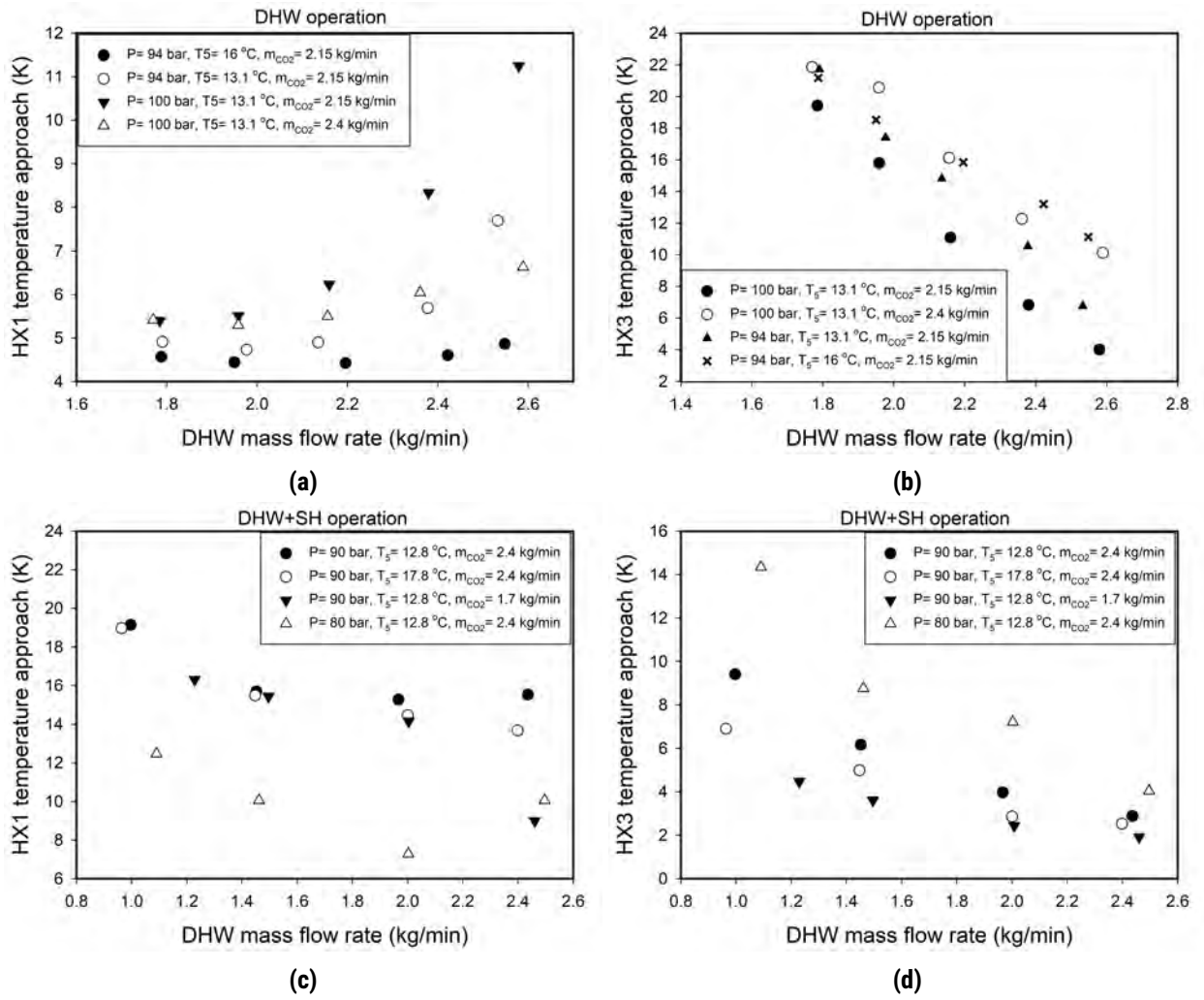

Figure 4.19: Temperature approach vs. DHW mass flow rate in (a,b) DHW operation and (c,d) DHW+SH operation.

rate of 11.6 kg/min, the temperature approach in both gas coolers decreases with the increase of DHW mass flow rate, resulting in some different trends than DHW operation. Specifically, Figure 4.19 (d) demonstrates that for the higher DHW water inlet temperature, temperature approach is lower for preheating gas cooler. As the system operates in DHW+SH mode, the CO_2 outlet temperature of the preheating gas cooler is lower and the slope of reduction with the increase of DHW mass flow rate is flatter than that of DHW mode, resulting in a different trend in the temperature approach with the increase of water inlet temperature.

Figure 4.20 (a) presents the results of SH gas cooler for the SH mode when the operating pressure is fixed at 90 bar, discharge temperature is 76 °C, and SH water inlet temperature is 35 °C, while Figure 4.20 (b) indicates the results for DHW+SH operation for gas cooler pressure of 85 bar, discharge temperature of 80 °C, DHW inlet temperature of 12.8 °C, SH inlet temperature of 30 °C, and DHW mass flow rate of 1.3 kg/min when the CO_2 and SH mass flow rates vary. The experimental results indicate that the SH gas cooler has been selected properly since the values are very low under SH operation and DHW+SH operation. In both operating modes, the temperature approach decreases when increasing SH mass flow rate and decreasing CO_2 mass flow rate.

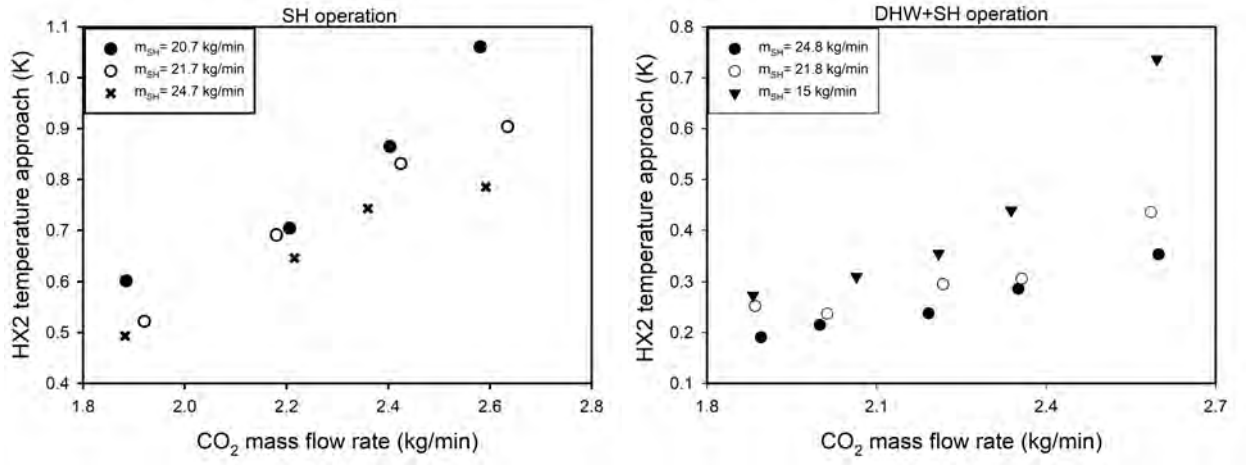

(a) **(b)**

Figure 4.20: HX2 temperature approach vs. CO_2 mass flow rate in (a) SH operation and (b) DHW+SH operation.

5 Correlation development for utilizing in TRNSYS

In this section, different correlations for current data are developed to predict the heat duty and supply temperature under different working conditions. The coefficient of determination, R^2, is calculated to evaluate the performance of each model and to select the most appropriate type of model. The excellent fit between the measured and predicted values would have R^2=1. Additionally, because of the complexity of the problem, the correlations developed with linear and quadratic model types failed due to a large error between the predicted and corresponding experimental data. Therefore, the Genetic Programming (GP) technique has been applied to develop non-linear equations. GP is a repetitive algorithm that approaches the answer step by step. GP algorithm combines equations and generates new equations. The implementation of the GP is described in Ref. [29].

The genetic programming is applied to 146 experimental data samples for both one-pass and two-pass heat exchangers and the following correlations are proposed to calculate the heat duty and supply temperature of DHW in the DHW and DHW+SH operations.

$$Q_{HX1} = 2.028 + 0.0002 \times m_{DHW} \times P^2 - 0.0004 \times P \times T_5 - 1.3E-06 \times P^3 \times cos(1.37E-03 \times T_{dis}^2) \times sin(tan(5.04E-05 \times m_{DHW} \times P^2)) \quad (5.1)$$

$$Q_{HX3} = 9.45 \times sqrt(m_{DHW}) + 2.32E-04 \times T_{dis}^2 \times cos(4 + 0.15 \times T_{dis} + 0.73 \times cos(1.45 \times T_{dis})) - 4.23 - 0.034 \times m_{DHW} \times P \quad (5.2)$$

$$T_{supply,DHW} = T_{dis} + 0.08 \times T_5 + 0.13 \times P \times m_{CO2} + 2.14 \times m_{DHW}^2 - 10.5 - 3.83 \times m_{CO2} - 0.21 \times T_{dis} \times m_{DHW} \quad (5.3)$$

where P, T_{dis}, T_5, and m_{DHW} are the inlet pressure, discharge temperature, water inlet temperature, and water mass flow rate, respectively. The correlations are validated when the 78.69<P (bar)<101.31, 68.11<T_{dis} (°C)<100.5, 0.96<m_{DHW} (kg/min)<2.89, and 10.48<T_5 (°C)< 20.01.

The SH heat duty and supply temperature correlations are proposed based on 163 experimental data samples collected in the SH and DHW+SH operating modes. The correlations are shown as:

$$Q_{HX2} = 5.68 + 1.21E-03 \times T_{dis} \times m_{CO2} \times m_{SH} + 4.91E-03 \times m_{SH}^2 \times sin(-1.08 \times T_{dis})^2 \times sin(0.366 \times T_{dis}) - sin(0.233 \times m_{SH}) \times cos(0.0049 \times m_{SH}^2 \times sin(0.366 \times T_{dis}) \times sin(-1.08 \times T_{dis})) - 0.14 \times T_8 \quad (5.4)$$

$$T_{supply,SH} = 1.76 \times m_{CO2} + 0.61 \times T_{dis} + 0.016 \times T_8^2 + \left(\frac{(3712.8 - 6957.8 \times (1.95E-02 \times T_8)^{m_{SH}})}{T_{dis}}\right) - 79.5 \quad (5.5)$$

where P, T_{dis}, T_8, and m_{SH} are the inlet pressure, discharge temperature, SH water inlet temperature, and SH mass flow rate, respectively. Above correlations are found to be reliable and robust when the

77.53779<P (bar)<91.65417, 68.1083<T_{dis} (°C)<93.21884, 10.18658<m_{SH} (kg/min)< 25.91105, and 23.18893<T_8 (°C)<36.5495.

The comparisons between the measured results and predicted results by the developed models in this study are shown in Figure 5.1. The values of R^2 for the reheating heat duty, space heating heat duty, preheating heat duty, DHW supply temperature, and SH supply temperature are 0.88, 0.86, 0.94, 0.99, and 0.94, respectively. The results show that the correlations perform very well in the prediction of heat duty and supply temperature.

The main advantages of the developed correlations in this study are the generality of the models for the considered operating modes (i.e., DHW, SH, and DHW+SH modes) and the capability of determining the influences of the operating parameters on the heat duty and supply temperature over a wide range. These equations are helpful in calculating the values of the supply temperatures and heat duties by assuming values of the operating parameters within valid ranges. These models are highly helpful for engineers involved in refrigeration research and they can be utilized to design and enhance the thermal performance of heat exchangers used in the transcritical carbon dioxide refrigerant system.

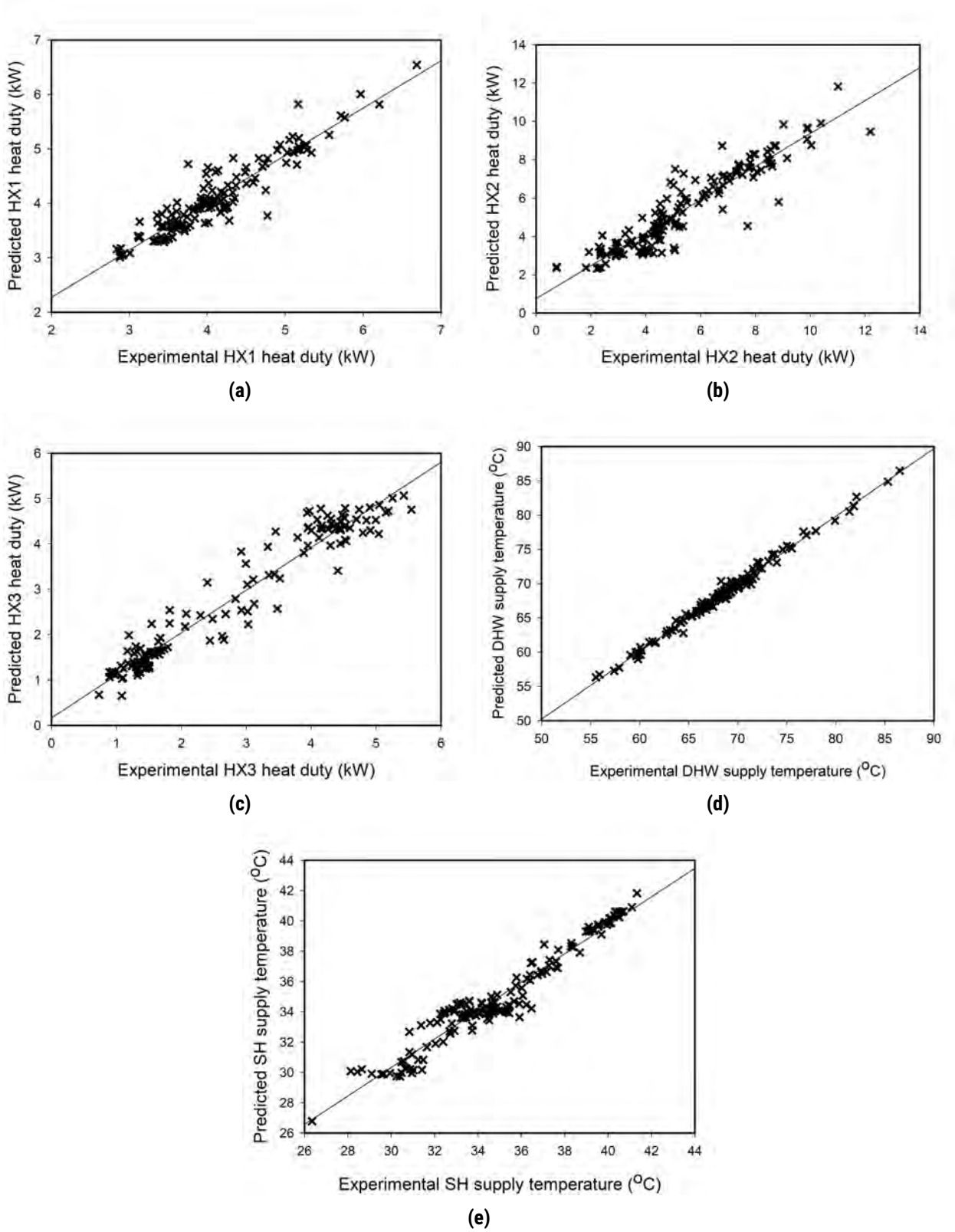

Figure 5.1: Comparison of calculated and experimental data.

6 RECOMMENDATION FOR GAS COOLER INSTALLATION

The difference between the DHW mass flow rate and SH mass flow rate makes some challenges to come up with a tri-partite gas cooler as a single unit. Figure 6 presents the most compact heat exchanger design and configuration for implementing into the second prototype. The advantages of this arrangement are:

- the two-pass gas coolers can be placed horizontally to facilitate the oil drain.
- it is a pretty compact solution that can be integrated with a frame and could be insulated all in one piece.
- all CO_2 connections to one side and DHW and SH connections to the opposite.

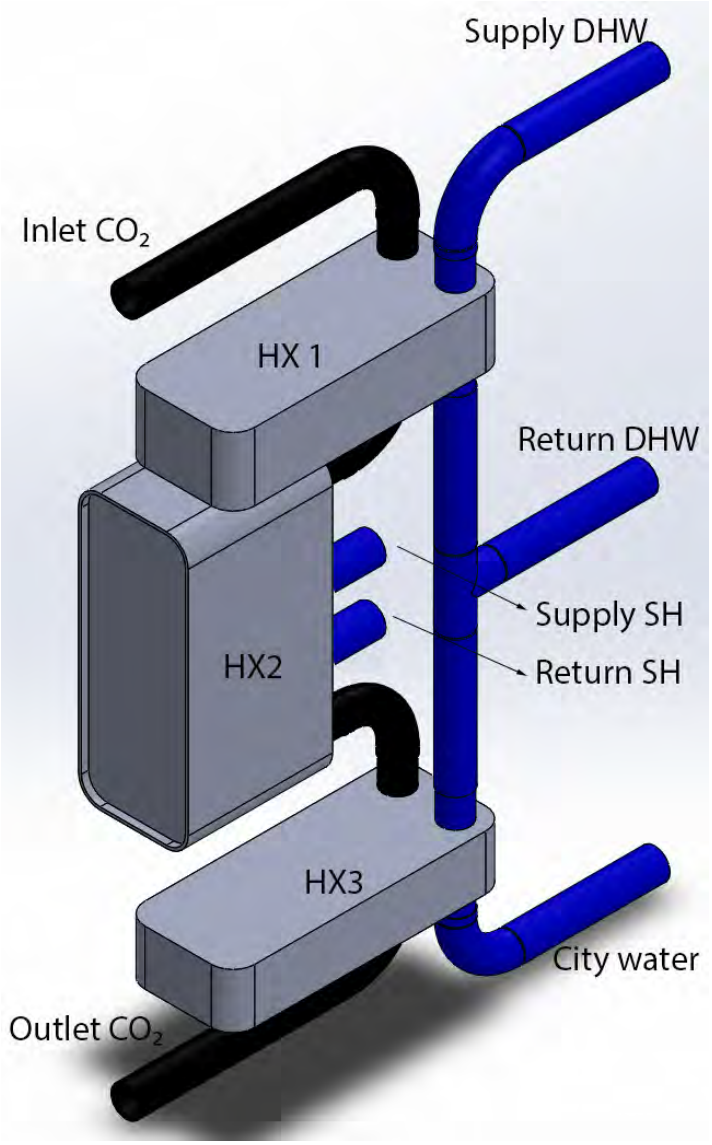

Figure 6.1: The 3D of compact tri-partite gas cooler configuration.

7 Concluding remarks

An experiment is conducted to investigate the performance of carbon dioxide (CO_2) in tri-partite brazed plate gas cooler in a steady-state transcritical heat pump water heater system using the CO_2-water test loop. The results are obtained for a system for only space heating, only hot water heating, and combined space heating and hot water heating. The gas cooler shows promising performance under the design conditions and is more compact than previous designs. The experimental results indicates that the brazed plate heat exchanger can be a promising technology for making transcritical CO_2 heat pumps reasonably efficient.

Furthermore, to provide a good insight into this study, a sensitivity analysis is carried out and the effects of different operating parameters on the total heat transfer coefficient, heat duty, pressure drop, supply temperature, and temperature approach are examined. The heat duty and supply temperature correlations for both space heating and domestic hot water cycles that include the effects of operating parameters are obtained by fitting the experimental data. The major remarkable conclusions of this analysis are obtained as follows:

- The total heat transfer coefficient drops with an increase in the gas cooler pressure in the liquid-like region, and it increases in the gas-like region due to different thermophysical properties of CO_2 under different pressures. The heat transfer reaches a maximum for a bulk temperature close to the pseudo-critical temperature due to the variation in the CO_2 thermodynamic properties including specific heat and thermal conductivity. The heat transfer coefficient enhances with an increase in the mass flow rate due to a rise in the Reynolds number and the diffusion rate. The larger the DHW water inlet temperature, the higher the total heat transfer coefficient in the liquid-like region, but no significant influence when CO_2 is in a high-temperature state.
- The higher average refrigerant temperature results in a lower average density and higher average velocity through the gas cooler, resulting in a higher pressure drop. At a given mass flow rate and gas cooler pressure, pressure drop increases with decreasing water inlet temperature, since as the inlet temperature increases, the viscosity decreases. The increase in the hot side fluid pressure can cause an increase in the density and thus a decrease in the velocity of CO_2, so the CO_2 side pressure drop decreases.
- The values of heat duty increases with the increases of water and CO_2 mass flow rates. The lower the water inlet temperature is, the higher the average heat duty is. The heat duty of DHW loop increases with an increase in the operating CO_2 pressure, while a higher operating CO_2 pressure leads to a lower SH heat duty under DHW+SH operation.
- The water outlet temperature increases as the mass flow rate of refrigerant increases and the water mass flow rate decreases. An increase of operating CO_2 pressure leads to a higher and lower value of DHW outlet temperature and SH outlet temperature, respectively. The supply temperature is higher at the higher water inlet temperature. The supply temperature is directly affected by the CO_2 inlet temperature as the gas coolers are designed to work in a counter-flow configuration.
- The higher water mass flow rate is recommended to decrease the temperature approach values under DHW, SH, and DHW+SH operations. The temperature approach also decreases with an increase of pressure and a decrease of CO_2 mass flow rate under DHW, SH, and DHW+SH operations. While a lower water inlet temperature is beneficial to lower the temperature approach of DHW operation, an opposite trend is demonstrated for DHW cycle under the DHW+SH operation.
- The values of the coefficient of determination exceeding 0.88, 0.86, 0.94, 0.99, and 0.94 for the reheating heat duty, space heating heat duty, preheating heat duty, DHW supply temperature, and SH supply temperature, respectively, demonstrate high reliability of the developed correlations in this study.

Bibliography

[1] A. Zendehboudi, A. Mota-Babiloni, P. Makhnatch, R. Saidur, and S. M. Sait, "Modeling and multi-objective optimization of an r450a vapor compression refrigeration system," *International Journal of Refrigeration*, vol. 100, pp. 141 – 155, 2019. [Online]. Available: http://www.sciencedirect.com/science/article/pii/S0140700719300088

[2] UNEP, "Report of the twenty-eighth meeting of the parties to the montreal protocol on substances that deplete the ozone layer, kigali," 2016. [Online]. Available: https://ozone.unep.org/treaties/montreal-protocol/amendments/kigali-amendment-2016-amendment-montreal-protocol-agreed

[3] C. Dang and E. Hihara, "In-tube cooling heat transfer of supercritical carbon dioxide. part 1. experimental measurement," *International Journal of Refrigeration*, vol. 27, no. 7, pp. 736 – 747, 2004, studies And Technologies Related To Ozone Depletion And Climate Change. [Online]. Available: http://www.sciencedirect.com/science/article/pii/S0140700704000817

[4] S. Riffat, C. Afonso, A. Oliveira, and D. Reay, "Natural refrigerants for refrigeration and air-conditioning systems," *Applied Thermal Engineering*, vol. 17, no. 1, pp. 33 – 42, 1997. [Online]. Available: http://www.sciencedirect.com/science/article/pii/1359431196000300

[5] G. Lorentzen and J. Pettersen, "A new, efficient and environmentally benign system for car air-conditioning," *International Journal of Refrigeration*, vol. 16, no. 1, pp. 4 – 12, 1993. [Online]. Available: http://www.sciencedirect.com/science/article/pii/014070079390014Y

[6] M.-H. Kim, J. Pettersen, and C. W. Bullard, "Fundamental process and system design issues in CO_2 vapor compression systems," *Progress in Energy and Combustion Science*, vol. 30, no. 2, pp. 119 – 174, 2004. [Online]. Available: http://www.sciencedirect.com/science/article/pii/S0360128503000765

[7] B. T. Austin and K. Sumathy, "Transcritical carbon dioxide heat pump systems: A review," *Renewable and Sustainable Energy Reviews*, vol. 15, no. 8, pp. 4013 – 4029, 2011. [Online]. Available: http://www.sciencedirect.com/science/article/pii/S1364032111002607

[8] F. Zhang, Y. Zhu, C. Li, and P. Jiang, "Thermodynamic optimization of heat transfer process in thermal systems using co2 as the working fluid based on temperature glide matching," *Energy*, vol. 151, pp. 376 – 386, 2018. [Online]. Available: http://www.sciencedirect.com/science/article/pii/S0360544218304079

[9] P. Nekså, H. Rekstad, G. Zakeri, and P. A. Schiefloe, "CO_2-heat pump water heater: characteristics, system design and experimental results," *International Journal of Refrigeration*, vol. 21, no. 3, pp. 172 – 179, 1998. [Online]. Available: http://www.sciencedirect.com/science/article/pii/S0140700798000176

[10] P. Nekså, "CO_2 heat pump systems," *International Journal of Refrigeration*, vol. 25, no. 4, pp. 421 – 427, 2002. [Online]. Available: http://www.sciencedirect.com/science/article/pii/S0140700701000330

[11] S. White, M. Yarrall, D. Cleland, and R. Hedley, "Modelling the performance of a transcritical CO_2 heat pump for high temperature heating," *International Journal of Refrigeration*, vol. 25, no. 4, pp. 479 – 486, 2002. [Online]. Available: http://www.sciencedirect.com/science/article/pii/S0140700701000214

[12] J. Stene, "Residential CO_2 heat pump system for combined space heating and hot water heating," *International Journal of Refrigeration*, vol. 28, no. 8, pp. 1259 – 1265, 2005, CO_2 as Working Fluid - Theory and Applications. [Online]. Available: http://www.sciencedirect.com/science/article/pii/S0140700705001775

[13] J. Sarkar, S. Bhattacharyya, and M. R. Gopal, "Simulation of a transcritical CO_2 heat pump cycle for simultaneous cooling and heating applications," *International Journal of Refrigeration*, vol. 29, no. 5, pp. 735 – 743, 2006. [Online]. Available: http://www.sciencedirect.com/science/article/pii/S014070070500263X

[14] S. Minetto, "Theoretical and experimental analysis of a CO_2 heat pump for domestic hot water," *International Journal of Refrigeration*, vol. 34, no. 3, pp. 742 – 751, 2011. [Online]. Available: http://www.sciencedirect.com/science/article/pii/S0140700710002938

[15] S. Wang, H. Tuo, F. Cao, and Z. Xing, "Experimental investigation on air-source transcritical CO_2 heat pump water heater system at a fixed water inlet temperature," *International Journal of Refrigeration*, vol. 36, no. 3, pp. 701 – 716, 2013. [Online]. Available: http://www.sciencedirect.com/science/article/pii/S014070071200271X

[16] Y. Zhu, Y. Huang, C. Li, F. Zhang, and P.-X. Jiang, "Experimental investigation on the performance of transcritical CO_2 ejector–expansion heat pump water heater system," *Energy Conversion and Management*, vol. 167, pp. 147 – 155, 2018. [Online]. Available: http://www.sciencedirect.com/science/article/pii/S0196890418304291

[17] S. Smitt, I. Tolstorebrov, and A. Hafner, "Integrated CO_2 system with hvac and hot water for hotels: Field measurements and performance evaluation," *International Journal of Refrigeration*, vol. 116, pp. 59 – 69, 2020. [Online]. Available: http://www.sciencedirect.com/science/article/pii/S0140700720301365

[18] J. Pettersen, A. Hafner, G. Skaugen, and H. Rekstad, "Development of compact heat exchangers for CO_2 air-conditioning systems," *International Journal of Refrigeration*, vol. 21, no. 3, pp. 180 – 193, 1998. [Online]. Available: http://www.sciencedirect.com/science/article/pii/S0140700798000139

[19] J. Sarkar, S. Bhattacharyya, and M. Gopal, "Optimization of a transcritical CO_2 heat pump cycle for simultaneous cooling and heating applications," *International Journal of Refrigeration*, vol. 27, no. 8, pp. 830 – 838, 2004. [Online]. Available: http://www.sciencedirect.com/science/article/pii/S0140700704000520

[20] J. Sarkar, S. Bhattacharyya, and M. Ram Gopal, "Irreversibility minimization of heat exchangers for transcritical CO_2 systems," *International Journal of Thermal Sciences*, vol. 48, no. 1, pp. 146 – 153, 2009. [Online]. Available: http://www.sciencedirect.com/science/article/pii/S1290072908000513

[21] B. M. Fronk and S. Garimella, "Water-coupled carbon dioxide microchannel gas cooler for heat pump water heaters: Part i - experiments," *International Journal of Refrigeration*, vol. 34, no. 1, pp. 7 – 16, 2011. [Online]. Available: http://www.sciencedirect.com/science/article/pii/S0140700710000903

[22] S. S. Pitla, E. A. Groll, and S. Ramadhyani, "Convective heat transfer from in-tube cooling of turbulent supercritical carbon dioxide: Part 2—experimental data and numerical predictions," *HVAC&R Research*, vol. 7, no. 4, pp. 367 – 382, 2001. [Online]. Available: https://www.tandfonline.com/doi/ref/10.1080/10789669.2001.10391281?scroll=top

[23] C.-H. Son and S.-J. Park, "An experimental study on heat transfer and pressure drop characteristics of carbon dioxide during gas cooling process in a horizontal tube," *International Journal of Refrigeration*,

vol. 29, no. 4, pp. 539 – 546, 2006. [Online]. Available: http://www.sciencedirect.com/science/article/pii/S0140700705002021

[24] Z.-B. Liu, Y.-L. He, Y.-F. Yang, and J.-Y. Fei, "Experimental study on heat transfer and pressure drop of supercritical co2 cooled in a large tube," *Applied Thermal Engineering*, vol. 70, no. 1, pp. 307 – 315, 2014. [Online]. Available: http://www.sciencedirect.com/science/article/pii/S1359431114003858

[25] T. Ma, W. xiao Chu, X. yang Xu, Y. tung Chen, and Q. wang Wang, "An experimental study on heat transfer between supercritical carbon dioxide and water near the pseudo-critical temperature in a double pipe heat exchanger," *International Journal of Heat and Mass Transfer*, vol. 93, pp. 379 – 387, 2016. [Online]. Available: http://www.sciencedirect.com/science/article/pii/S0017931015010145

[26] G.-W. Zhang, P. Hu, L.-X. Chen, and M.-H. Liu, "Experimental and simulation investigation on heat transfer characteristics of in-tube supercritical co2 cooling flow," *Applied Thermal Engineering*, vol. 143, pp. 1101 – 1113, 2018. [Online]. Available: http://www.sciencedirect.com/science/article/pii/S135943111830526X

[27] Y. Zhu, Y. Huang, S. Lin, C. Li, and P. Jiang, "Study of convection heat transfer of co2 at supercritical pressures during cooling in fluted tube-in-tube heat exchangers," *International Journal of Refrigeration*, vol. 104, pp. 161 – 170, 2019. [Online]. Available: http://www.sciencedirect.com/science/article/pii/S014070071930132X

[28] E. W. Lemmon, , I. H. Bell, M. L. Huber, and M. O. McLinden, "NIST Standard Reference Database 23: Reference Fluid Thermodynamic and Transport Properties-REFPROP, Version 10.0, National Institute of Standards and Technology," 2018. [Online]. Available: https://www.nist.gov/srd/refprop

[29] S. Hosseini, M. Moradkhani, M. Valizadeh, A. Zendehboudi, and M. Olazar, "A general heat transfer correlation for flow condensation in single port mini and macro channels using genetic programming," *International Journal of Refrigeration*, 2020. [Online]. Available: http://www.sciencedirect.com/science/article/pii/S0140700720302760

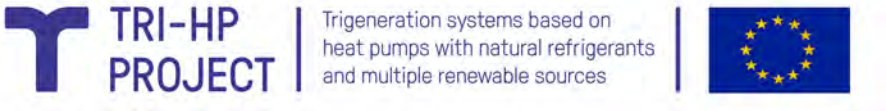

This project has received funding from the European Union's Horizon 2020 research and innovation programme under grant agreement N. 814888.
The sole responsibility for the content of this paper lies with the authors. It does not necessarily reflect the opinion of the European Commission (EC). The EC is not responsible for any use that may be made of the information it contains.

©TRI-HP PROJECT. All rights reserved.

Any duplication or use of objects such as diagrams in other electronic or printed publications is not permitted without the author's agreement.